materials

MDPI

Article

Smart Magnetic Drug Delivery System for Targeted, Intracellular Delivery of Irinotecan and Platinum-Based Antitumoral Drugs

Ludmila Motelica [1,2,3], Bogdan Stefan Vasile [1,2,3], Denisa Ficai [1,3,4,*], Ovidiu-Cristian Oprea [1,3,4], Vasile-Adrian Surdu [5], Roxana Doina Trusca [1], Angela Spoiala [1,2], Geanina Voicu [6], Maria Anghelache [6], Daciana Silvia Marta [7], Victor-Eduard Peteu [7,8], Anton Ficai [1,3,8] and Manuela Calin [6]

1 National Centre for Micro and Nanomaterials & National Centre for Food Safety, Faculty of Chemical Engineering and Biotechnologies, National University of Science and Technology Politehnica Bucharest, Spl. Independentei 313, 060042 Bucharest, Romania; ludmila.motelica@upb.ro (L.M.); bogdan.vasile@upb.ro (B.S.V.); ovidiu.oprea@upb.ro (O.-C.O.); roxana_doina.trusca@upb.ro (R.D.T.); angela.spoiala@upb.ro (A.S.); anton.ficai@upb.ro (A.F.)
2 Advanced Research Center for Innovative Materials, Products and Processes, National University of Science and Technology Politehnica Bucharest, 060042 Bucharest, Romania
3 Academy of Romanian Scientists, 3 Ilfov Street, 050045 Bucharest, Romania
4 Department of Inorganic Chemistry, Physical Chemistry and Electrochemistry, Faculty of Chemical Engineering and Biotechnologies, National University of Science and Technology Politehnica Bucharest, 1-7 Gh Polizu Street, 050054 Bucharest, Romania
5 Department of Materials Science, Faculty of Materials Science and Engineering, Transilvania University of Brasov, 29 Eroilor Blvd., 500036 Brasov, Romania; vasile.surdu@unitbv.ro
6 "Medical and Pharmaceutical Bionanotechnologies" Department, Institute of Cellular Biology and Pathology "N. Simionescu", B.P. Hasdeu 8, 050568 Bucharest, Romania; geanina.voicu@icbp.ro (G.V.); anghelache.maria@icbp.ro (M.A.); manuela.calin@icbp.ro (M.C.)
7 Ultrastructural Pathology and Bioimaging Laboratory, "Victor Babes" National Institute of Pathology, 99-101 Splaiul Independentei, 050096 Bucharest, Romania; daciana.marta@ivb.ro (D.S.M.); peteuvictoreduard@gmail.com (V.-E.P.)
8 Department of Science and Engineering of Oxide Materials and Nanomaterials, Faculty of Chemical Engineering and Biotechnologies, National University of Science and Technology Politehnica Bucharest, 1-7 Gh Polizu Street, 011061 Bucharest, Romania
* Correspondence: denisa.ficai@upb.ro

Abstract

Coated magnetic nanoparticles (MNPs) comprising Fe_3O_4 are a powerful drug delivery system for cancer treatment. They can be preferentially internalized into the tumour cells and release the antitumoral agents on-site. In the present work, we have functionalized the MNPs with glutamic acid which, even if non-essential, is strongly involved in the protein synthesis as a nitrogen donor, being used as a conjugate for specific antitumoral drugs due to its capability to internalize into tumour versus healthy cells faster. The functionalized MNPs were stabilized by polyethylene glycol (PEG) coating. This system improves drug efficacy by concentrating therapeutic agents at the tumour site, and can also induce ferroptosis in cancer cells, an iron-dependent cell death process, which has a beneficial therapeutic effect. Additionally, PEG molecules on the surface of MNPs facilitate drug conjugation for targeted delivery to cancer cells. These MNPs were designed as a delivery system for antitumoral drugs like irinotecan, carboplatin and cisplatin for personalized therapies. Based on the obtained results, it was found that the functionalization with glutamic acid and stabilization with PEG can improve the internalization efficiency of the magnetic carriers into the tumour cells. Owing to their stability, the MNPs can reach and penetrate mitochondria and organize around lipid vesicles, with the most effective results observed for the cisplatin-loaded system from a concentration of 0.1 mg/mL.

Academic Editors: David Sánchez-García and Katarzyna Winnicka

Received: 11 November 2025
Revised: 10 February 2026
Accepted: 22 February 2026
Published: 27 February 2026

Keywords: drug delivery; magnetic nanoparticles; glutamic acid; antitumoral agents; personalized treatment; cisplatin; carboplatin; irinotecan

1. Introduction

A significant increase in the global burden of early-onset cancer was observed between 1990 and 2019, with incidence rising by 79.1% and mortality by 27.7%. While the disproportionate rise in incidence relative to mortality suggests advancements in detection and management, early-onset cancer remains a critical global public health challenge. In 2019, the highest mortality was associated with cancers of the breast, trachea, bronchus and lung, and stomach, as well as colorectal cancer. Analysis of incidence trends revealed the most rapid increases for nasopharyngeal and prostate cancers, whereas early-onset liver cancer incidence demonstrated the sharpest decline. Early-onset colorectal cancer was particularly notable for its disease burden, ranking among the top five causes of disability-adjusted life years (DALYs) for both sexes. Geographically, the highest burden was observed in high–middle- and middle-Sociodemographic Index (SDI) regions. Morbidity was positively correlated with SDI, while mortality rates decreased substantially as SDI increased beyond 0.7. Projection models estimate a continued rise, forecasting a 31% increase in global incidence and a 21% increase in deaths from early-onset cancer by 2030 [1].

The side effects of anticancer drugs currently used in cancer treatment, such as resistance developed over time, but also cytotoxicity and unwanted secondary metabolites formed during current treatments, represent major disadvantages that have led to the need to develop personalized treatments based on the combination of immunotherapy, photo-thermal therapy and adjuvant therapy with nano-formulated natural drugs [2].

Due to their unique properties (such as high biocompatibility, high saturation magnetization, possibility of targeting an organ by applying a magnetic field, increased circulation time in vivo and non-toxicity), magnetic nanoparticles (MNPs) have been extensively studied as potential anti-cancer systems, being successfully used in the diagnosis and treatment of cancer [3].

MNPs with dimensions ranging from ~10 to ~200 nm are considered safe and suitable for permeabilizing the tumour cell membrane. It has been demonstrated that by judicious choice of the synthesis method, nanoparticles with optimal dimensions and properties can be obtained. These MNPs will further ensure proper transport of drugs to target cancer cells for diagnosis and treatment through suitable controlled release over a desired period, thus increasing the efficacy and compatibility with the target. At the same time, targeted therapy minimizes the unwanted systemic toxicity induced by conventional chemotherapy (Figure 1). Cancer development is fast and thus the blood vessels are developed in a shorter time and have imperfections, and thus the nanoparticles can easily leak from these vessels and reach the tumours, even at larger sizes (up to 100–200 nm, which is not usual in the case of the normal vessels). Along with the size, the shape and the surface chemistry of the magnetic nanoparticles are extremely important, and often these characteristics can be associated with the synthesis routes and conditions, and this is why many synthesis methods are researched, including green synthesis and biological syntheses using bacterial strains [2,4,5].

Bare magnetic nanoparticles such as Fe_3O_4 and Fe_2O_3 are easily recognized by the animal/human immune system upon reaching blood circulation, where they are shortly resorbed, thus strongly limiting their clinical use. To overcome this major shortcoming, magnetic Fe_3O_4 nanoparticles are stabilized/functionalized with different agents, depending on the desired application. Stabilizing agents such as chitosan, poly-lactic-co-glycolic

acid (PLGA) or polyethylene glycol (PEG) prevent early resorption and aggregation in plasma [6] and increase bioavailability in the desired cells, tissues and organs. Furthermore, the use of PEG as a stabilizing agent for magnetic nanoparticles increases their water dispersibility, enhances their colloidal stability and internalization capability, and, thus, increases the potential for anticancer therapy. In addition, PEGylation allows the surface modification of the Fe_3O_4-MNP core and release of anticancer drugs, such as paclitaxel, doxorubicin, curcumin, quercetin, and cisplatin, for targeted drug delivery [7–9]. Therefore, the synthesis of MNPs with polymer coatings is more suitable for effective drug delivery in oncology therapy (Figure 2) [10,11]. Many research groups used amino acids such as glycine, arginine, lysine and tyrosine to induce suitable functional groups on the surface of MNPs for biomedical applications. Amino acids, which are also used as stabilizing agents to prevent the formation of magnetic aggregates, can in turn be efficient in the transport of specific antitumoral drugs into the tumour cells. Dutta et al., for instance, present the effect of some antitumoral agents conjugated with glutamic acid, highlighting the benefits regarding their transport and internalization into the tumour cells. Some of the chemotherapeutic agents presented in this review are paclitaxel, cisplatin, curcumin, all-trans retinoic acid, 20(s)-camptothecin, etc. [12,13].

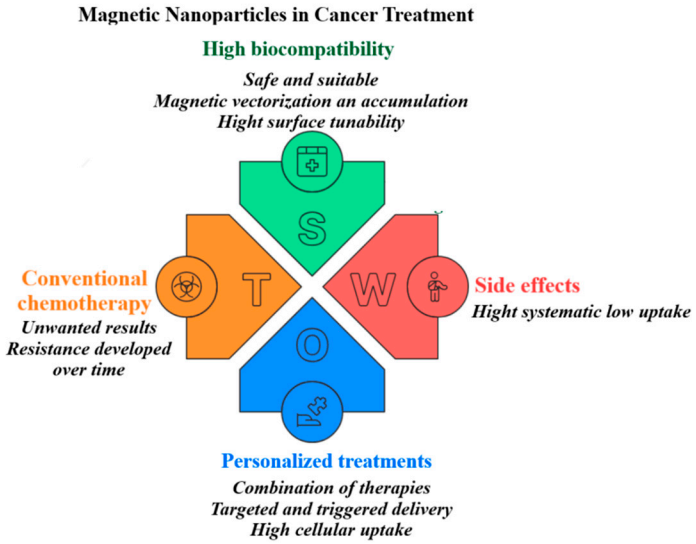

Figure 1. The applications of magnetic nanoparticles in cancer treatment.

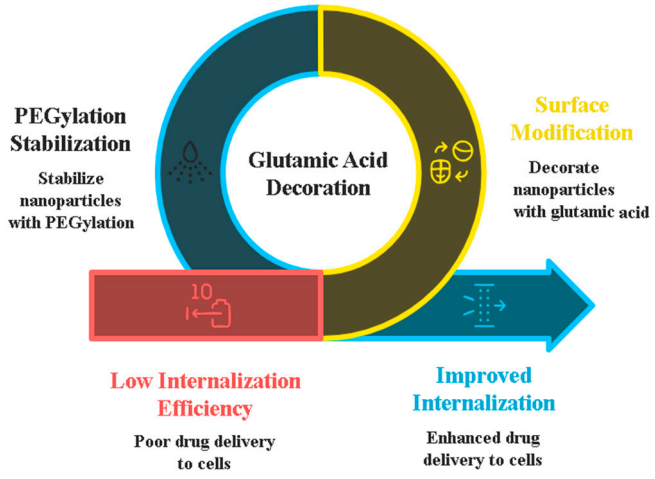

Figure 2. Enhancing drug delivery in cancer therapy with glutamic acid.

In this study, we have coated PEGylated magnetic nanoparticles with glutamic acid (Glu) to obtain the above-mentioned effects, not directly for the antitumoral drugs but

for the magnetic carrier itself, these carriers being used to transport and release platinum-based cytostatics (cisplatin and carboplatin) as well as irinotecan. Therefore, the starting hypothesis is that MNPs coated with glutamic acid will be preferentially internalized in the tumour cells (in a targeted way) compared with the non-tumour cells. Once these carriers are inside the tumour cells, release can occur, assuring a high efficiency and low systemic toxicity. Further, magnetic triggering will be tested to ensure even more efficient cancer therapy.

2. Materials and Methods

Magnetite nanoparticles (Figure 3) were obtained using the following materials: iron (III) chloride—$FeCl_3$ 99% (Sigma Aldrich, Darmstadt, Germany); iron chloride (II) tetrahydrate—$FeCl_2 \cdot 4H_2O$ 99% (Merck, Darmstadt, Germany); and sodium hydroxide—NaOH (Sigma Aldrich). For stabilization, PEG-8000 was used, and for functionalization, glutamic acid (Sigma) was chosen. As antitumoral agents, cisplatin (Sigma), carboplatin (Sigma) and irinotecan (Aldrich) were used. In all syntheses, distilled water was used. All reagents were used without any further purification.

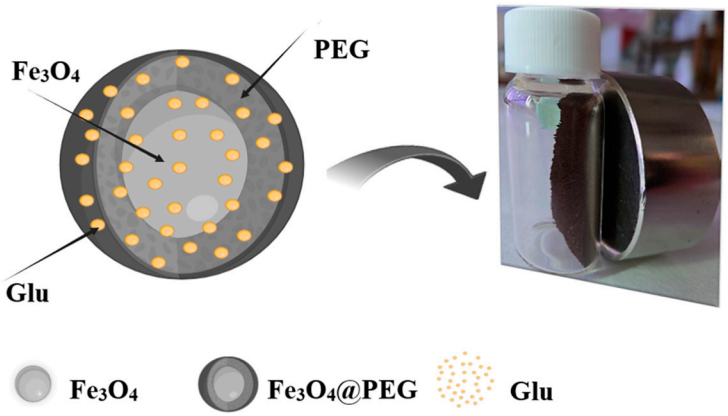

Figure 3. Depiction of the PEG-stabilized magnetic nanoparticles functionalized with glutamic acid (glutamate).

2.1. Cell Culture

The antitumoral activity of cytostatic drug-loaded Fe_3O_4 NPs stabilized with PEG and functionalized with glutamic acid was investigated using a human hepatocarcinoma (HepG2) cell line purchased from the American Type Culture Collection (ATCC, Manassas, VA, USA). The cells were grown in Dulbecco's modified Eagle medium with 4.5 g/L glucose (Sigma-Aldrich, Merck KGaA, Darmstadt, Germany), supplemented with 10% fetal bovine serum, 100 units/mL penicillin, and 100 µg/mL streptomycin (complete medium), in an incubator at 37 °C, 5% CO_2. Cells were sub-cultivated at a ratio of 1:4 (ATCC recommendation).

2.2. Preparation and Optimization of Fe_3O_4_Glu

The Fe_3O_4_Glu nanoparticles were obtained using the co-precipitation method presented in our previous work [12] (Scheme 1).

Briefly, in a Berzelius flask, 200 mL of distilled water was added, in which 5 g of Glu and 25 g of NaOH were dissolved. A second solution was obtained by dissolving 8.70 g of $FeCl_2 \cdot 4H_2O$ and 14.2 g of $FeCl_3$ in 50 mL water. The second solution was added dropwise under continuous stirring over the initial alkaline solution while a black precipitate appeared. The obtained suspension was stirred for another 3 h. The obtained black precipitate was washed several times until pH = 7 was obtained and no more chloride

ions were identified. The obtained precipitate was dried at 50 °C in an oven. A summary of the precursors and combination ratios used for the preparation of the magnetic nanopowder is presented in Table 1.

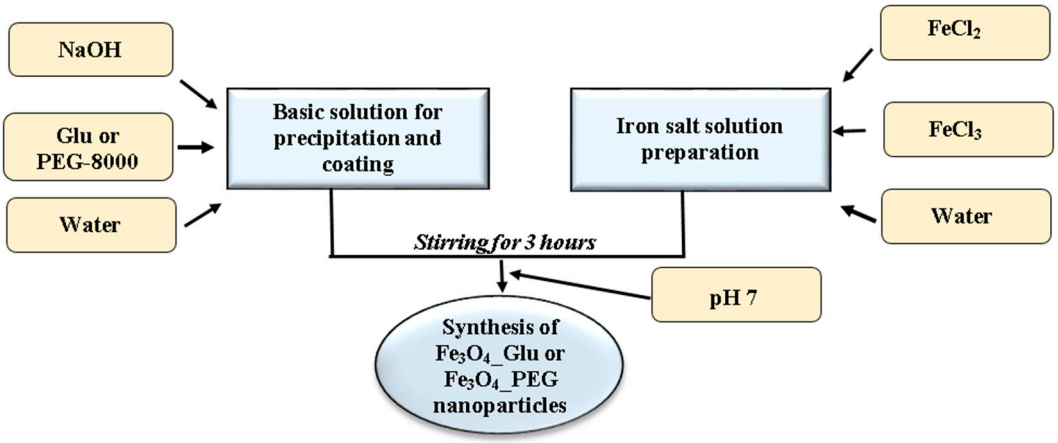

Scheme 1. Preparation of the Fe_3O_4_Glu or Fe_3O_4_PEG nanoparticles.

Table 1. Preparation of the multifunctional magnetic nanomaterials.

Sample	$FeCl_2 \cdot 2H_2O$ (g)	$FeCl_3$ (g)	Glu (g)	PEG (g)
Fe_3O_4	8	14	-	-
Fe_3O_4_Glu	8	14	5	
Fe_3O_4_PEG	8	14		50
Fe_3O_4_PEG_Glu	8	14	5	50

2.3. Preparation and Optimization of Fe_3O_4_PEG

Similarly, as above, a basic solution was obtained from 20 g of NaOH, 50 g of PEG-8000 and 200 mL of distilled H_2O, in a Berzelius flask. To this solution, we added 50 mL from the second solution (containing the iron precursors) dropwise, under continuous stirring, until a black precipitate appeared. The obtained solution was stirred for another 3 h. The obtained black precipitate was washed several times until pH = 7 was obtained and no more chloride ions were identified. Finally, the precipitate was dried at 50 °C in an oven [12].

2.4. Preparation and Optimization of Fe_3O_4_PEG_Glu

Similarly, as above, a basic solution was obtained from 20 g of NaOH, 5 g of Glu, 50 g of PEG-8000 and 200 mL of distilled H_2O, in a Berzelius flask (Table 1). To the basic solution, we added 50 mL of the second solution (containing the iron precursors) dropwise, under continuous stirring, until a black precipitate appeared. The obtained solution was stirred for another 3 h. The obtained black precipitate was washed several times until pH = 7 was obtained and no more chloride ions were identified. Finally, the precipitate was dried at 50 °C in an oven [12].

In all cases, the purification step is the most challenging. Successive magnetic decantation and washing on a filter lead to some material losses, but the overall yield remains ~70% for all the samples. At this level, there is no visible difference from the point of aggregation during the synthesis and purification step but, after drying, the crushing and dispersing of the dried magnetic component are visibly different.

2.5. Loading of MNPs with Antitumoral Agents—Irinotecan (Irotec), Carboplatin (CarboPt) and Cisplatin (CisPt)

The magnetic nanoparticles were loaded by contacting them with the acetone solution of the antitumor drug. A solution obtained from 5 mL acetone and 0.1 g of the antitumor drug (cisplatin, carboplatin or irinotecan) was added to 1 g of magnetic nanoparticles, and the mixture was ground in a mortar until the complete evaporation of the solvent was achieved. Subsequently, the pestle, the weighing vial and the mortar walls were washed with another 5 mL of acetone, and the solution was added over the magnetite, and the mortar process was repeated until complete evaporation. The whole washing process was performed 4 times to improve the recovery of the antitumor drug from the instruments and ensure a better absorption of the antitumor drug on the surface of the MNPs [12]. A summary of the compositions to obtain the MNPs loaded with cytostatics is presented in Table 2.

Table 2. Loading of multifunctional magnetic materials.

Sample	MNPs (g)	Cisplatin (g)	Carboplatin (g)	Irinotecan (g)
Fe_3O_4_Glu_CisPt	1	0.1		
Fe_3O_4_Glu_CarboPt	1		0.1	
Fe_3O_4_Glu_Irinotecan	1			0.1
Fe_3O_4_PEG_Glu_CisPt	1	0.1		
Fe_3O_4_PEG_Glu_CarboPt	1		0.1	
Fe_3O_4_PEG_Glu_Irinotecan	1			0.1

MNPs = bare or PEGylated magnetic nanoparticles (Fe_3O_4, Fe_3O_4_PEG, Fe_3O_4_Glu or Fe_3O_4_PEG_Glu.

2.6. Characterization Methods

Specific physicochemical methods were employed for the characterization of the obtained MNPs. X-ray diffraction patterns (XRD) were recorded on a PANalytical X'Pert Pro MPD analyser (PANalytical, Almelo, The Netherlands) using Cu-Kα radiation. Rietveld refinement was executed using a Caglioti function for peak width, a pseudo-Voigt function for peak profile and a polynomial function for background approximation.

A Thermo Nicolet iS50 FTIR spectroscope (Thermo Fisher Scientific, Waltham, MA, USA) equipped with an ATR module was used to record the FTIR spectra in the range of 4000–400 cm^{-1} with a resolution of 4 cm^{-1}. Each spectrum was obtained by averaging 32 scans.

Scanning electron microscopy (SEM) images were recorded using a Quanta Inspect F (FEI, Hillsboro, OR, USA) microscope equipped with an EDS spectrometer, the samples being covered with a thin film of silver. The images were recorded using an Everhart–Thornley Detector (ETD) operating at an acceleration voltage of 30 kV.

Transmission Electron Microscopy (TEM) images were obtained on fine powder samples using the G2 F30 S-TWIN, Tecnai FEI High-Resolution Transmission Microscope (HRTEM) (Thermo Fisher Scientific, Waltham, MA, USA). The images were obtained using transmission mode at 300 kV with a point resolution of 1 Å.

A Netzsch STA 449 °C Jupiter device (Netzsch, Selb, Germany) was used for the thermal analysis via TG-DSC. The heating speed was 10 °C·min^{-1} up to 900 °C, under the flow of dried air at 50 mL min^{-1}.

2.7. Cytotoxicity Assessment

2.7.1. Colorimetric Assay

To evaluate the viability of HepG2 cells after exposure to MNPs, an XTT assay was performed. The method used was reported in our work [12]. The assay measures the

metabolic activity of cells by conversion of the yellow tetrazolium salt of XTT (2,3-Bis-(2-methoxy-4-nitro-5-sulfophenyl)-2H-tetrazolium-5-carboxyanilide salt) to orange-coloured formazan compounds. The HepG2 cells were seeded in 96-well culture plates at a density of 1×10^4 cells/well and allowed to adhere for 24 h. The cells were incubated with different concentrations of drug-loaded MNPs functionalized with glutamic acid (10, 100, and 500 µg/mL) in a complete medium without L-glutamine. Corresponding concentrations of free drugs (carboplatin, irinotecan, and cisplatin), namely 1, 10, and 50 µg/mL, were also used. To assess the influence of surface modifications, four types of magnetic nanoparticles (MNPs) were used as controls: plain MNPs, glutamic acid-functionalized MNPs, PEGylated MNPs, and PEGylated MNPs functionalized with glutamic acid. Before use, the powdered MNPs were sterilized via UV exposure for 5 min. The sterilized particles were then re-suspended in complete culture medium and subjected to sonication in a water bath for 10 min to ensure homogeneous dispersion before cell incubation. After 24 h of exposure, the culture medium was collected, and the cells were incubated with XTT/PMS (phenazine methosulfate) reagent prepared in phenol red-free DMEM. Following a 2 h incubation at 37 °C, the optical absorbance of the orange solution was measured at 450 nm using an Infinite® M200 PRO spectrophotometer (Tecan, Männedorf, Switzerland). Data were normalized to untreated control cells and presented as mean percentages from two independent experiments, each conducted in duplicate.

2.7.2. Bioluminescent Assay

The metabolic activity of HepG2 was further assessed by measuring the adenylate kinase (AK) released from the damaged cells following treatment with various MNP formulations, using the ToxiLight™ Cytotoxicity BioAssay Kit (cat. no. LT17-217, Lonza Bioscience, Basel, Switzerland) [12]. After 24 h of cell incubation with varying concentrations of drug-loaded MNPs or the corresponding concentration of free drug (as above), the medium was collected for AK quantification via bioluminescent detection (Berthold technology Mithras LB 940, Berthold Technologies, Oak Ridge, TN, USA). The data were normalized to values obtained for untreated cells, considered as 1, and expressed as the mean ± S.D. (standard deviation) of two experiments performed in duplicate.

2.7.3. Live/Dead Cell Assay

After 24 h of HepG2 cell exposure to 100 µg/mL of drug-loaded MNPs (corresponding drug-loaded concentration is 10 µg/mL) or 10 µg/mL of free drugs (carboplatin, irinotecan, or cisplatin), cell viability was assessed using the Live/Dead assay kit by staining with Calcein-AM and propidium iodide (PI) (SIGMA-Aldrich, Merck KGaA, Darmstadt, Germany) [14]. Following staining, live cells exhibited green fluorescence from Calcein-AM, while dead cells emitted red fluorescence due to PI uptake. Fluorescence imaging was conducted at 10× magnification using an Olympus IX81 inverted microscope (Olympus, Tokyo, Japan) equipped with filter sets optimized for FITC and Texas Red channels.

2.7.4. Uptake of MNPs by Hepatocarcinoma Cells

The Prussian Blue staining method was used to investigate the internalization of MNPs by HepG2 cells. Cells were seeded in 96-well plates at a density of 1×10^4 cells/well and allowed to adhere for 24 h. Subsequently, they were incubated for an additional 24 h with various drug-loaded MNP formulations, as previously described. At the end of the incubation period, cells were gently washed with phosphate-buffered saline (PBS) to remove non-internalized nanoparticles and digested overnight at 37 °C with 20% hydrochloric acid (HCl). Following digestion, 5% potassium ferrocyanide ($K_4[Fe(CN)_6]$) solution was added to each well to develop the characteristic blue coloration [15]. The absorbance of the resulting Prussian Blue complex was measured at 700 nm using an Infinite® M200 PRO

spectrophotometer (Tecan, Männedorf, Switzerland). Quantification was performed by comparison to a standard curve generated from known concentrations of Fe_3O_4, and results were expressed as mean ± standard deviation (S.D.) from two independent experiments conducted in duplicate.

To visualize internalized magnetic nanoparticles (MNPs), HepG2 cells were fixed in 4% paraformaldehyde (PFA) for 15 min at room temperature. Cells were then incubated for 10 min with a freshly prepared 1:1 solution of 5% potassium ferrocyanide ($K_4[Fe(CN)_6]$) and 20% hydrochloric acid (HCl), enabling Prussian Blue staining for iron detection before optical microscopy analysis. After washing with phosphate-buffered saline (PBS), cells were stained with eosin Y (Sigma-Aldrich, Merck KGaA, Darmstadt, Germany) for 10 min. Microscopic examination was then performed using an Olympus CKX41 inverted microscope.

The internalization of the various types of MNPs (stabilized or not with PEG and functionalized or not with Glu) and loaded with the above mentioned antitumoral drugs was evaluated using traditional light microscopy as well as Transmission Electron Microscopy, using the G2 F30 S-TWIN, Tecnai FEI High-Resolution Transmission Microscope (HRTEM). The microscope was operated in transmission mode at 300 kV with a point resolution of 1 Å. The preparation of the samples for recording the images was carried out under the conditions presented in Table 3.

Table 3. Preparation conditions of the samples for recording the images.

Samples Containing Cells Suspended in a Fluid Are Included in Agar to Have the Necessary Consistency for Subsequent Inclusion in Epoxy Resin:	**Specification**
the sample is fixed: fixative is added over the cells in the culture medium so that the final concentration of the fixing solution is 2.5% (glutaraldehyde in TCS with sucrose)	RT, 2–2½ h
the sample in the fixative is centrifuged	1.250 rpm/15 min, 4 °C
re-suspend the cell pellet in 0.1 M TCS	4 °C, 10 min
it is centrifuged	1.250 rpm/15 min, 4 °C
it is suspended in 0.1 M TCS	4 °C, 10 min
it is centrifuged	1.250 rpm/15 min, 4 °C
post-fixation with 0.1 M osmium tetra oxide in 0.2 M TCS	4 °C, 30 min
it is centrifuged	3.000 rpm/15 min, 4 °C
the test in 0.1 M TCS is suspended	4 °C, 10 min
it is centrifuged	3.000 rpm/15 min, 4 °C
the test in 0.1 M TCS is suspended	4 °C, 10 min
at this moment the process can be interrupted	24 h
it is centrifuged	3.000 rpm/15 min, 4 °C
suspend the pellet in a drop of warm 1% agar	
put in the refrigerator until the agar hardens	4 °C, 20 min
cut the sample included in the agar into 1 mm^3 fragments	-
immerse the fragments in 0.1 M TCS	4 °C 10 min
dehydration ethyl alcohol 30°	4 °C 15 min
dehydration ethyl alcohol 50°	4 °C 15 min
dehydration ethyl alcohol 70°	4 °C 15 min
dehydration ethyl alcohol 90°	4 °C 15 min
dehydration ethyl alcohol 96°	RT 15 min
dehydration ethyl alcohol 100°	RT 2 × 15 min
propylene oxide	RT 3 × 10 min

Table 3. *Cont.*

Samples Containing Cells Suspended in a Fluid Are Included in Agar to Have the Necessary Consistency for Subsequent Inclusion in Epoxy Resin:	Specification
bath I: propylene oxide/epoxy resin (2/1)	RT 1–2 h
bath II: propylene oxide/epoxy resin (1/2)	RT overnight
bath III: epoxy resin in uncovered containers (to evaporate the rest of the propylene oxide)	RT 2-3 h
inclusion in a drop of freshly prepared epoxy resin in labelled plastic capsules	RT
epoxy resin polymerization	60 °C 24 h
filling the capsules with epoxy resin	RT
epoxy resin polymerization	60 °C 24 h
remove the blocks from the plastic capsules and put them in a box with a lid	The boxes are labelled with the sample number

RT—room temperature; TCS—cacodylate buffer working solution; rpm—rotations per minute; h—hour.

3. Results and Discussions

The X-ray diffractograms (Figure 4) recorded on Fe_3O_4 and Fe_3O_4 stabilized with glutamic acid prove the obtainment of Fe_3O_4 NPs as the only crystalline phase. The XRD diffractograms recorded on Fe_3O_4 and Fe_3O_4 stabilized with glutamic acid and synthesized show six peaks at 18.96, 30.18, 35.61, 43.26, 57.4, 62.8 and 69.3, corresponding to 111, 220, 311, 222, 422, 511 and 440 respectively, specific to a pure cubic structure with space group Fd-3ms [12].

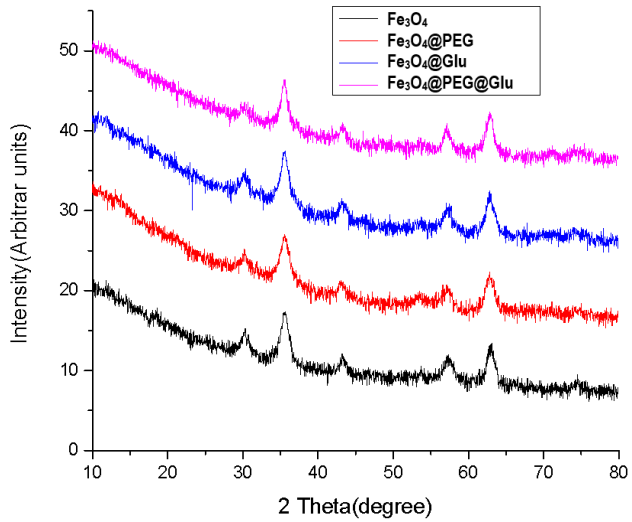

Figure 4. XRD pattern of MNPs.

In the XRD diffractograms recorded on the materials, Fe_3O_4_PEG and Fe_3O_4_PEG_Glu, it can be observed that the loading with PEG and glutamic acid does not change the crystalline structure of magnetite but induces a slight decrease in the intensity of the peaks characteristic of Fe_3O_4.

Using Rietveld refinement, the lattice parameters were determined (Table 4). The average crystallite size was calculated to be 10 nm from XRD peak broadening (Scherer equation).

Based on literature data, all the FTIR spectra recorded on the magnetic materials Fe_3O_4, Fe_3O_4_PEG, Fe_3O_4_Glu, Fe_3O_4_PEG_Glu, Fe_3O_4_PEG_Glu_CarboPt, Fe_3O_4_PEG_Glu_CisPt, and Fe_3O_4_PEG_Glu_Irinotecan present the Fe-O band characteristic of magnetite structure and peaks assigned to -OH, -NH_2 and -COOH functional groups of PEG and glutamic acid.

The IR spectra recorded on the as-synthesized uncoated Fe_3O_4 MNPs (Figure 5) showed metal–oxygen bands at 537 cm^{-1}, attributed to the intrinsic stretching vibrations of the metal–oxygen bond in tetrahedral geometry (Fe_{tetra}-O), while the metal–oxygen band observed at 420 cm^{-1} is attributed to the intrinsic stretching vibrations of the metal–oxygen bond in (Fe_{octa}-O) geometry [16]. The peak at 859 cm^{-1} corresponds to Fe–O stretching vibration.

Table 4. Lattice parameters were calculated using Rietveld refinement.

Characteristic	Fe_3O_4_Glu	Fe_3O_4_PEG	Fe_3O_4_PEG_Glu
COD #	96-900-9769	96-900-9769	96-900-9769
System	Cubic	Cubic	Cubic
Space group	Fd-3m	Fd-3m	Fd-3m
a (Å)	8.358547 ± 0.005338	8.401285 ± 0.007402	8.368488 ± 0.005285
V (Å^3)	583.9725	592.9761	586.0586
R_{exp}	16.81584	16.1714	17.48735
R_p	7.56886	7.98225	7.67825
R_{wp}	10.36828	11.37559	10.62435
GOF	0.38017	0.49483	0.36911
Crystallinity (%)	10.84	8.84	9.06
Crystallite size, <D> (nm)	5.87 ± 0.47	5.53 ± 0.67	7.76 ± 1.69
Micro-strain <S> (%)	1.71 ± 0.92	1.87 ± 1.10	1.42 ± 0.98

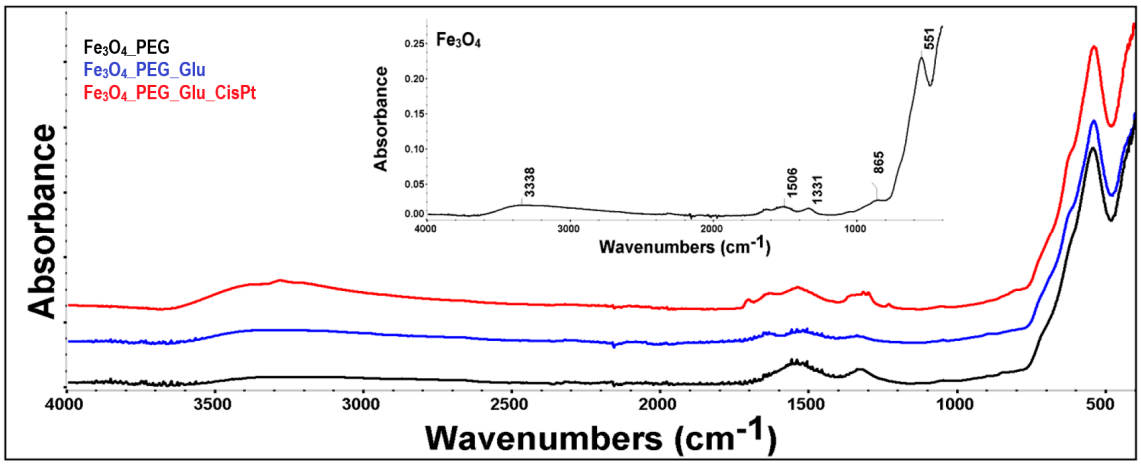

Figure 5. FTIR spectra of Fe_3O_4, Fe_3O_4_PEG, Fe_3O_4_PEG_Glu, and Fe_3O_4_PEG_Glu_CisPt.

In the FTIR spectra recorded on the nanoparticles of Fe_3O_4_PEG, Fe_3O_4_PEG_Glu and Fe_3O_4_PEG_Glu_CisPt (Figure 5), the bands corresponding to core MNPs around the values of 537 and 623 cm^{-1} can be identified, which are attributed to the Fe-O bond in the octahedral and tetrahedral geometry, but also the bands characteristic of the functional groups -COOH, -NH_2, -OH in the Glu and PEG. The peaks from 1653 and 3448 cm^{-1} can be attributed to the -OH groups in the Glu and PEG, but also to the water adsorbed on the surface, which confers a highly hydrophilic character to the surface, essential in biomedical applications. The absorption bands appearing in the range of 1000–1700 cm^{-1} are characteristic of the functional groups in the Glu structure, but also for PEG. The stretching vibrational bands assigned to the COO- groups of the glutamic acid (υ_{asim} and υ_{sim}) appear at a higher wavenumber in the spectra of Fe_3O_4_Glu or Fe_3O_4_PEG_Glu

(1652 cm^{-1} and 1653 cm^{-1} respectively), compared to the spectrum of pure glutamic acid (1632 cm^{-1}) (Figure 5), which may prove the existence of a conjugation effect of the carboxyl groups with the Fe ions of the Fe_3O_4 MNPs. Literature reports [6,12,17] indicate that because Glu is a bidentate molecule, the COO- moieties exhibit a strong affinity towards iron ions.

In addition, the absorption bands at 1090 cm^{-1} (–C–O–C–) and 1470 cm^{-1} are attributed to the stretching vibration of the C–C group of PEG [18–20] (Figure 6). The absorption peak at 741 cm^{-1} in the Fe_3O_4_PEG spectrum can be attributed to the strong bending vibrations of the 1,2-C–H bonds, and the absorption peak at 841 cm^{-1} corresponds to the bending vibrations of the 1,4-disubstituted or 1,2,3,4-tetrasubstituted C–H bond. All these bands confirmed the existence of PEG in the product [16].

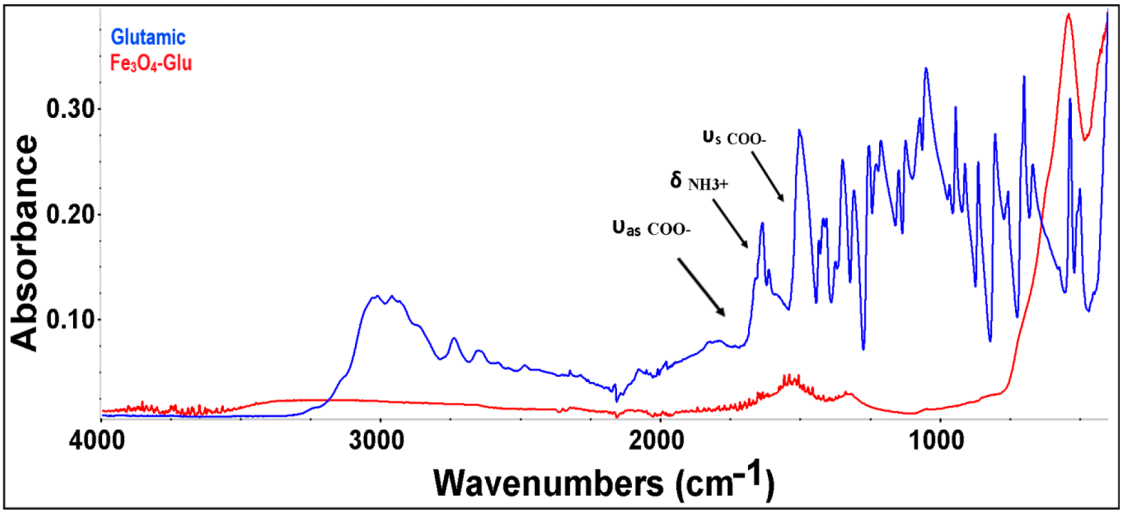

Figure 6. FTIR spectra of Fe_3O_4_Glu and glutamic acid.

Additionally, the bands appearing in the spectra recorded on PEG-coated MNPs were found to be weaker than those of pure nanoparticles. Therefore, the FTIR spectra showed the existence of van der Waals interactions between the PEG chain and the Fe_3O_4 nanoparticles in the polymeric environment.

The FTIR spectrum of Fe_3O_4_PEG_Glu_Cisplatin (Figure 7) presents a broader and more intense band in the 3200–3400 cm^{-1} region due to the N–H bonds from cisplatin. At the same time, specific irinotecan peaks like carbonyl C=O stretching vibration can be observed for the Fe_3O_4_PEG_Glu_Irinotecan sample at 1735 cm^{-1}.

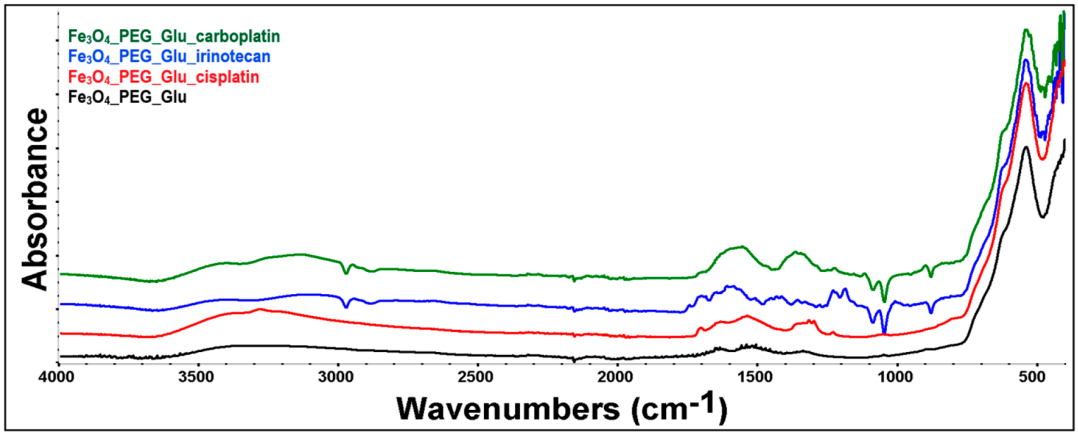

Figure 7. FTIR spectra of Fe_3O_4_PEG_Glu, Fe_3O_4_PEG_Glu_Cisplatin, Fe_3O_4_PEG_Glu_Carboplatin, and Fe_3O_4_PEG_Glu_Irinotecan.

3.1. SEM Analysis

The particle dimensions and morphology of synthesized MNPs (Fe_3O_4, Fe_3O_4_PEG, Fe_3O_4_Glu, Fe_3O_4_PEG_Glu) were studied using scanning electron microscopy analysis. SEM images recorded on uncoated Fe_3O_4 MNPs indicate fine particles with regularly spherical morphology, with sizes between 10 and 15 nm (Figure 8). SEM images recorded on Fe_3O_4_PEG, Fe_3O_4_Glu, and Fe_3O_4_PEG_Glu MNPs indicate the same regularly spherical morphology but dimensions around 6–9 nm.

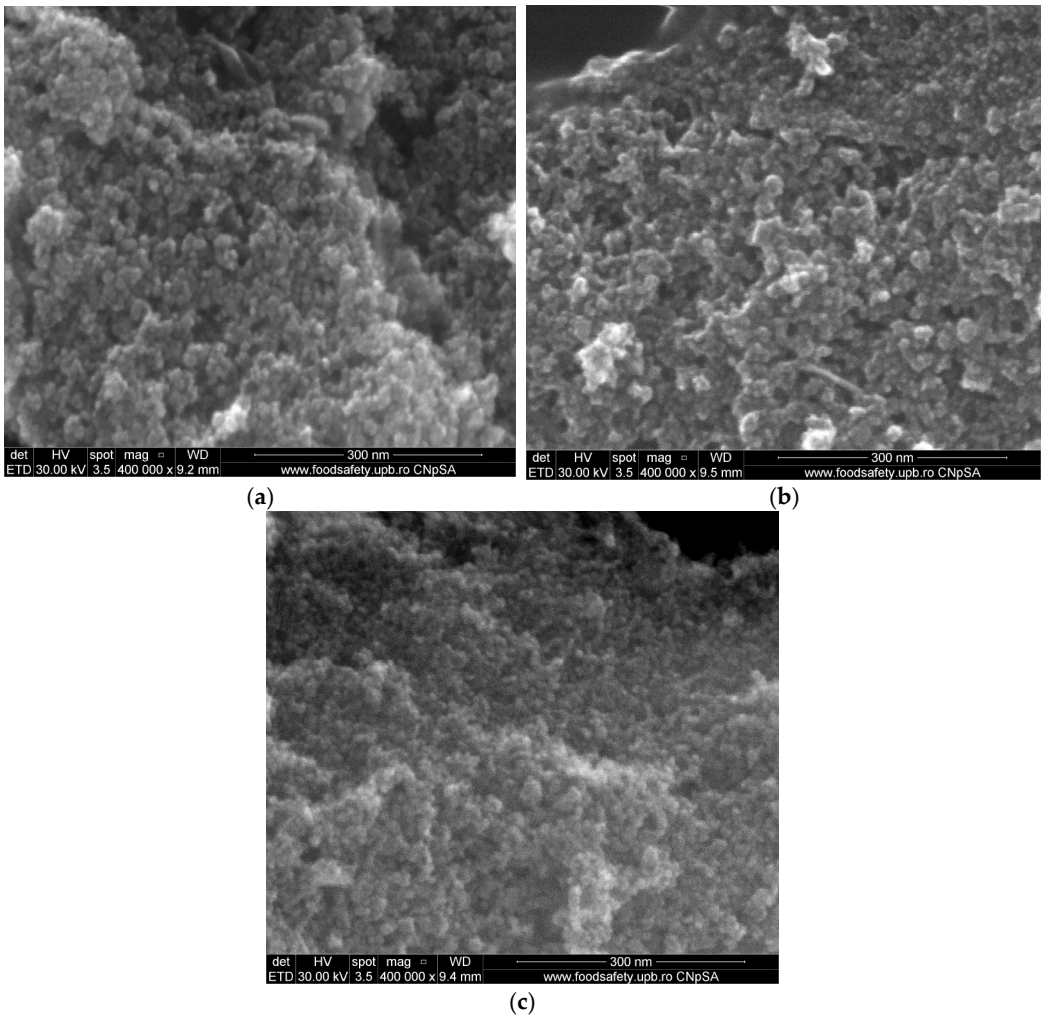

Figure 8. SEM images for (**a**) Fe_3O_4_Glu, (**b**) Fe_3O_4_PEG, (**c**) Fe_3O_4_PEG_Glu.

This observation showed that the PEG surfactant and/or glutamic acid may absorb selectively onto facets of crystallites, which may inhibit the free growth of Fe_3O_4 nanoparticles [16].

3.2. TEM Analysis

The details of the microstructure of the synthesized powders were evaluated by TEM (Figure 9). According to the TEM images (Figure 9a), the uncoated Fe_3O_4 MNPs exhibited a strong agglomeration effect, due to the increase in the attractive forces between the particles, resulting from the increase in the surface-to-volume ratio. From the TEM images (Figure 9a) recorded on the uncoated Fe_3O_4 NPs, a spherical or nearly spherical shape with a relatively uniform particle size (10 nm) distribution can be observed. The average size of coated nanoparticles was found to be 15–20 nm, while the surface morphology and form remained constant (Figure 9b–d). These sizes are proper for medical applications, while the PEG coating can confer the proper stabilization and internalization [6].

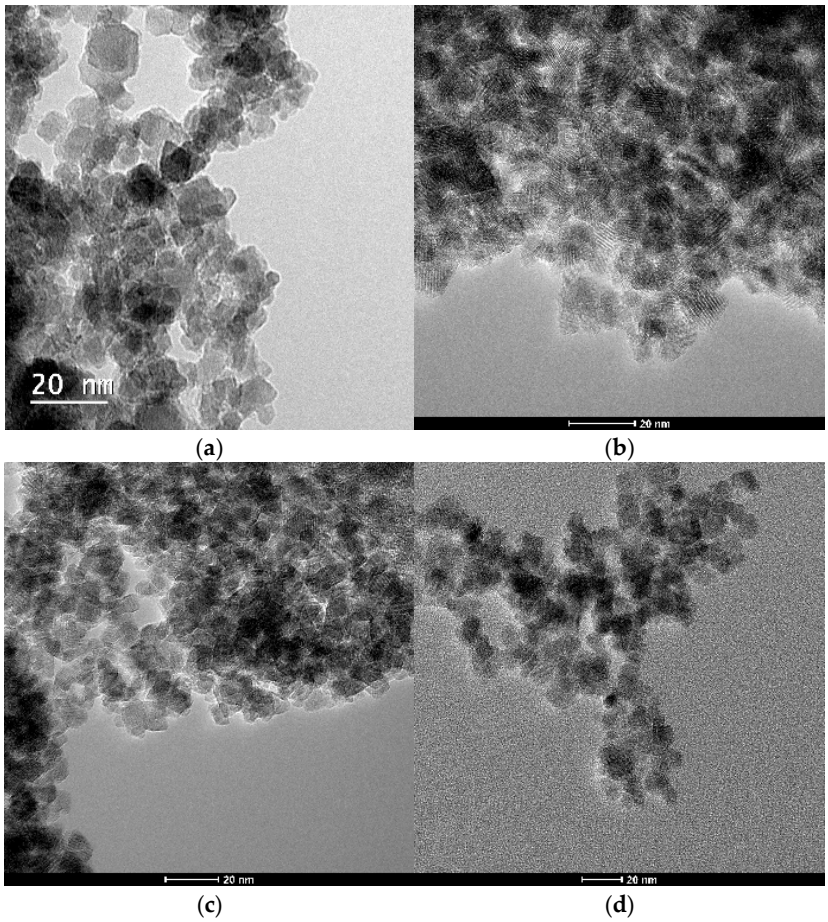

Figure 9. TEM images for (**a**) Fe_3O_4 NPs, (**b**) Fe_3O_4_Glu, (**c**) Fe_3O_4_PEG, (**d**) Fe_3O_4_PEG_Glu.

The thermal analyses for the Fe_3O_4, Fe_3O_4_PEG, Fe_3O_4_Glu, and Fe_3O_4_PEG_Glu samples are presented in Figure 10. The results from thermal analysis reveal three mass loss steps. From room temperature up to 200 °C, the samples exhibit a mass loss (~0.65–3.46%), with an associated endothermic effect with a peak around ~80–90 °C. In this stage the dehydration of the samples occurs [21].

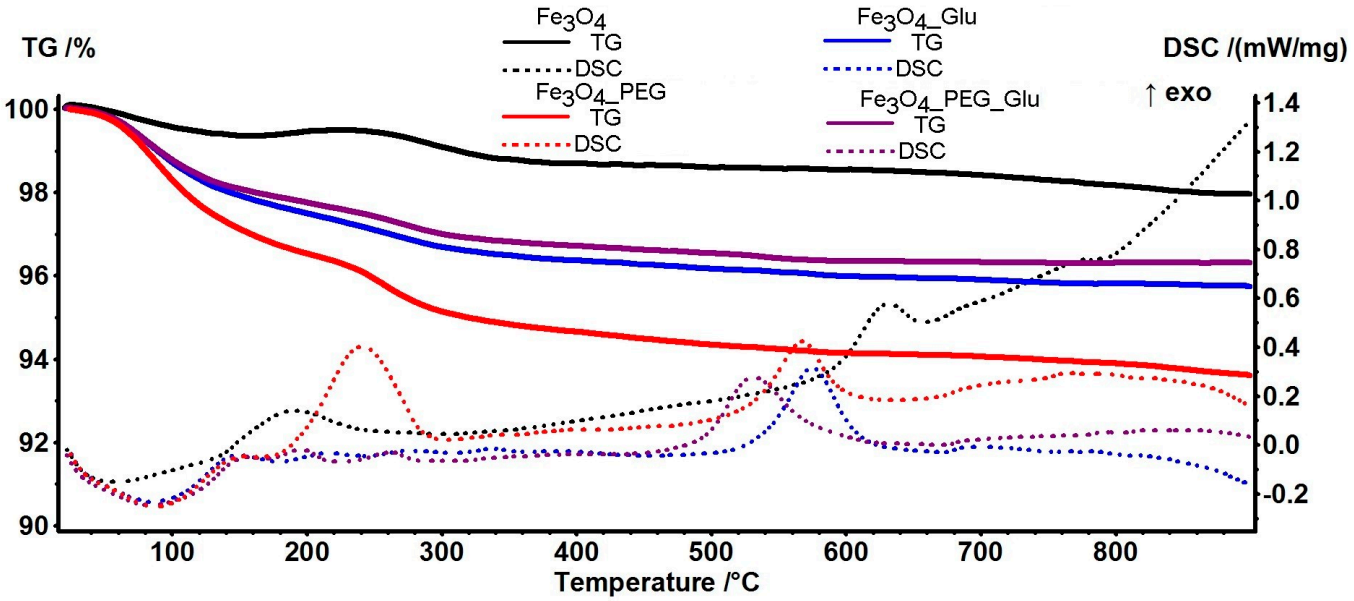

Figure 10. The TG and DSC curves for simple and functionalized MNP samples.

From 200 °C to 400 °C, the mass of the samples decreases by ~0.66–1.88%. This process can be assigned to the incomplete oxidation and thermal decomposition of the PEG and Glu molecules from the surface of nanoparticles. Around this temperature the Fe^{2+} ions are transformed to Fe^{3+}, by oxidation, the magnetite being transformed into maghemite (γ-Fe_2O_3) [22]. The effects on the DSC curve suggest that in this temperature interval several reactions of oxidation and degradation by fragmentation occur. After 400 °C the residual carbonaceous mass is completely oxidized. Noticeably, around 550–630 °C an exothermic effect can be observed, which is characteristic of the phase transition of maghemite to hematite (γ-Fe_2O_3 to α-Fe_2O_3) [12,23]. Whenever the magnetite nanoparticles are protected by an inert outer layer (like silica), the oxidation reaction of Fe^{2+} cannot occur, and maghemite is not obtained, so the exothermic effect is detected [24]. In Table 5 we display the principal numeric data from the thermal analyses together with the estimated load (calculated from residual mass).

Table 5. Principal data obtained from thermal analysis.

Sample	Mass Loss RT-200 °C	Mass Loss 200–400 °C	Residual Mass (%)	Estimated Load * (%)
Fe_3O_4	0.65%	0.66%	97.96%	-
Fe_3O_4_Glu	2.50%	1.13%	95.75%	0.26% *
Fe_3O_4_PEG	3.46%	1.88%	93.61%	2.49% *
Fe_3O_4_PEG_Glu	2.24%	1.04%	96.31%	0.71% *
Fe_3O_4_PEG_Glu_CisPt	3.43%	3.15%	89.31%	22.36% **
Fe_3O_4_PEG_Glu_CarboPt	1.88%	4.65%	91.84%	10.22% **
Fe_3O_4_PEG_Glu_Irinotecan	2.74%	8.98%	86.40%	10.29% **

* organic content vs. Fe_3O_4 and ** drug load vs. Fe_3O_4_PEG_Glu.

The thermal analyses for the MNPs loaded with antitumoral drugs are presented in Figure 11.

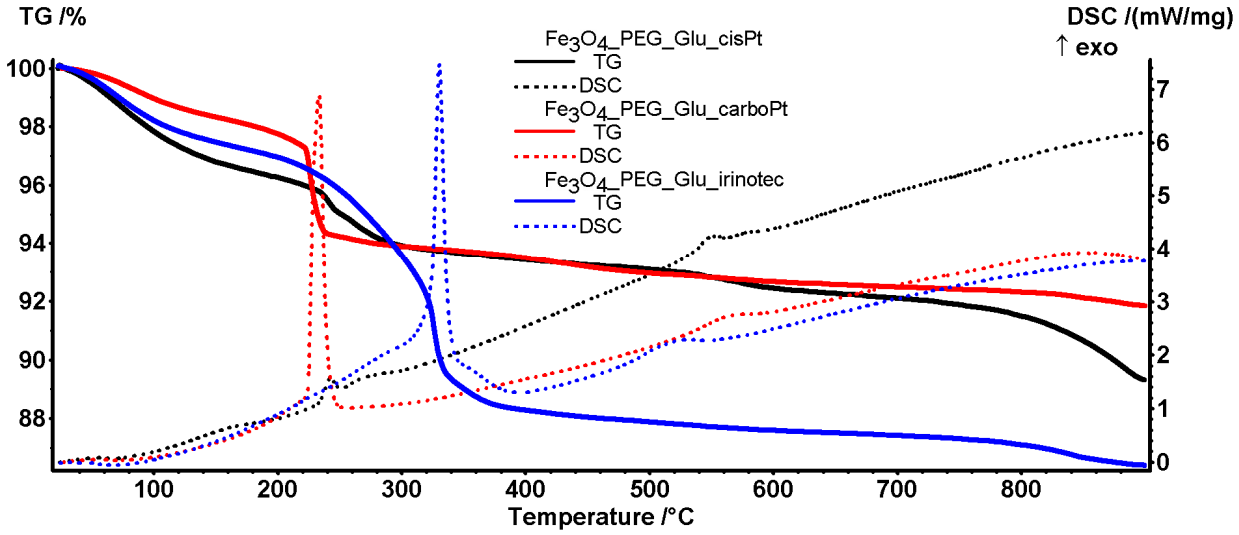

Figure 11. The TG and DSC curves for Fe_3O_4_PEG_Glu_CisPt, Fe_3O_4_PEG_Glu_CarboPt and Fe_3O_4_PEG_Glu_Irinotecan samples.

The antitumoral drugs loaded on the surface of the MNPs generate noticeable differences in thermal behaviour. Firstly, up to 200 °C, the samples exhibit a small mass loss

(~1.88–3.43%) assigned to the elimination of the weakly bounded solvent molecules. The associated endothermic effect reaches its minimum at ~63–73 °C.

The main thermal event can be observed in the temperature interval 200–400 °C. The oxidative degradation leads to a mass decrease of ~3.15–8.98% (Table 5). The associated effect on the DSC curve is exothermic for all samples, but the shape and position are specific to the antitumoral drug loaded on the MNPs. In the case of CisPt the exothermic effect is weak, around 239 °C, due to its lack of organic parts, but for CarboPt and Irinotecan the exothermic effects are strong and sharp with maxima at 231.8 °C and 320.3 °C, respectively. Moreover, for Irinotecan, due to its organic nature, the exothermic effect has a broad base indicating multiple oxidation processes.

A slower mass loss, assigned to the oxidation of the residual carbonaceous mass, can be observed after 400 °C, up to 800 °C when a minor step is evident. The weak exothermic effect observable around ~530–553 °C is assigned to the physical transformation of γ-Fe_2O_3 to α-Fe_2O_3 [25,26].

3.3. Evaluation of the Cytotoxic Effects of Drug-Loaded Magnetic Nanoparticles in HepG2 Cells

The cytotoxic effects of glutamic acid-functionalized magnetic nanoparticles (MNPs) loaded with anticancer drugs were evaluated in HepG2 cells following 24 h of incubation. Cells were exposed to MNPs at concentrations of 10, 100, and 500 μg/mL, corresponding to drug payloads of 1, 10, and 50 μg/mL, respectively. For comparison, equivalent concentrations of free drugs (CisPt, Irinotecan and CarboPt) were also tested under identical conditions. Across all tested concentrations, control MNPs, including plain MNPs, PEGylated MNPs, glutamic acid-functionalized MNPs, and PEGylated MNPs functionalized with glutamic acid, showed no detectable cytotoxicity in HepG2 cells, as illustrated in Figure 12 (left panel). The cellular viability was significantly reduced in a dose-dependent manner after cells' incubation with cisplatin-loaded MNPs, especially in the case of PEGylated MNPs (Figure 12A). Incubation with 10 μg/mL Fe_3O_4_Glu_CisPt and Fe_3O_4_PEG_Glu_CisPt, corresponding to an encapsulated CisPt concentration of 1 μg/mL, resulted in enhanced anti-tumour activity, significantly reducing HepG2 cells' viability by ~30% and 40%, respectively, compared to untreated control cells. At the same concentration (1 μg/mL), free cisplatin reduced HepG2 cell viability by approximately 15%; however, this effect was not statistically significant. At a loaded cisplatin concentration of 10 μg/mL (corresponding to 100 μg/mL of MNPs), both Fe_3O_4_PEG_Glu_CisPt and free cisplatin significantly reduced HepG2 cell viability by approximately 60%.

In contrast, Fe_3O_4_Glu_CisPt induced only a ~30% reduction in viability under the same conditions, relative to untreated control cells. At a cisplatin-equivalent concentration of 50 μg/mL (corresponding to 500 μg/mL of MNPs), Fe_3O_4_Glu_CisPt and Fe_3O_4_PEG_Glu_CisPt reduced HepG2 cell viability by approximately 60–65%. In contrast, free cisplatin at the same concentration induced a markedly higher cytotoxic effect, reducing cell viability by ~90% relative to untreated controls. For carboplatin, a dose-dependent cytotoxic response was observed, with 500 μg/mL of MNPs (equivalent to 50 μg/mL encapsulated carboplatin) resulting in a ~40% decrease in cell viability (Figure 12B). Instead, free CarboPt induced a reduction in cell viability by ~ 50% regardless of the concentration. Irinotecan-loaded MNPs (Fe_3O_4_PEG_Glu_Irinotecan) had a greater dose-dependent anti-tumour activity compared to free Irinotecan (Figure 12C). At 10 μg/mL of Fe_3O_4_PEG_Glu_Irinotecan, corresponding to 1 μg/mL encapsulated Irinotecan, the HepG2 viability decreased by ~40% compared to untreated cells, while the same concentration of free Irinotecan did not influence the cell viability. Higher concentrations of MNPs and free Irinotecan reduced the cell viability at a similar percentage, by ~50%

at 100 µg/mL Fe_3O_4_PEG_Glu_Irinotecan and 10 µg/mL free Irinotecan, and by ~75% at 500 µg/mL Fe_3O_4_PEG_Glu_Irinotecan and 50 µg/mL free Irinotecan.

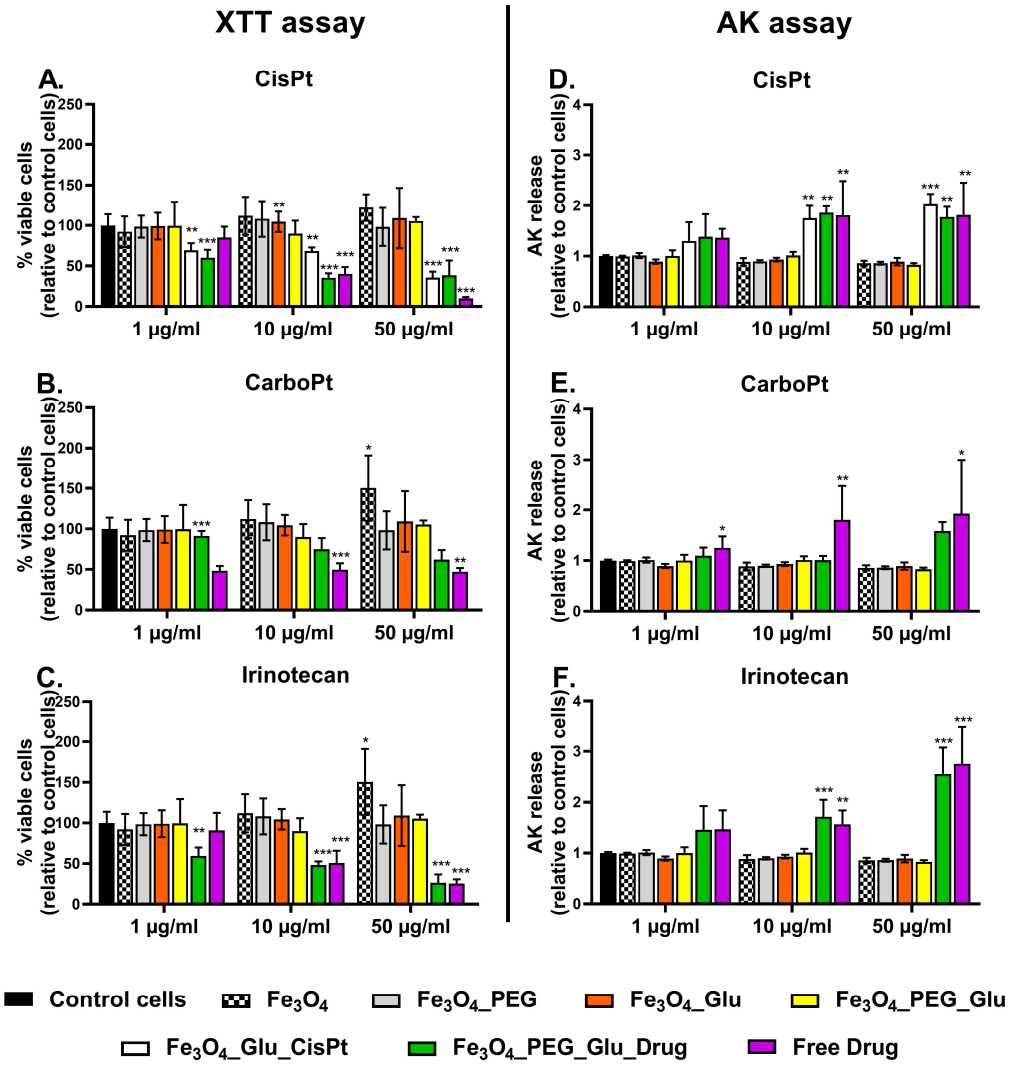

Figure 12. Cytotoxicity evaluation of drug-loaded MNPs and free drugs in HepG2 cells. Left panel (**A**–**C**): XTT assay performed after 24 h of incubation with three concentrations of MNP formulations (10, 100, and 500 µg/mL) and corresponding concentrations of free drugs investigated: (**A**) Cisplatin (CisPt), (**B**) Carboplatin (CarboPt), (**C**) Irinotecan. Right panel (**D**–**F**): Quantification of adenylate kinase (AK) released from damaged HepG2 cells using the ToxiLight assay, following 24 h of incubation with the same MNP formulations and corresponding free drug concentrations: (**D**) CisPt, (**E**) CarboPt, (**F**) Irinotecan. Statistical significance: * $p < 0.05$, ** $p < 0.01$, *** $p < 0.001$ versus control cells.

Adenylate kinase (AK) release from damaged HepG2 cells was quantified using the ToxiLight™ assay. The results mirrored the XTT assay, confirming that magnetic nanoparticles (MNPs) lacking encapsulated drugs did not affect cell viability (Figure 12, right panel). A significantly higher release of AK was observed when HepG2 cells were treated with 100 and 500 µg/mL MNPs, corresponding to 10 and 50 µg/mL of encapsulated CisPt (Figure 12D). Comparable levels of AK release were observed for 10 and 50 µg/mL of free CisPt. Consistent with the viability assay results, calcein-AM/propidium iodide (PI) staining revealed similar cytotoxic effects in HepG2 cells (Figure 13) following 24 h exposure to 100 µg/mL of Fe_3O_4_Glu_CisPt and Fe_3O_4_PEG_Glu_CisPt MNPs, corresponding to 10 µg/mL of encapsulated cisplatin.

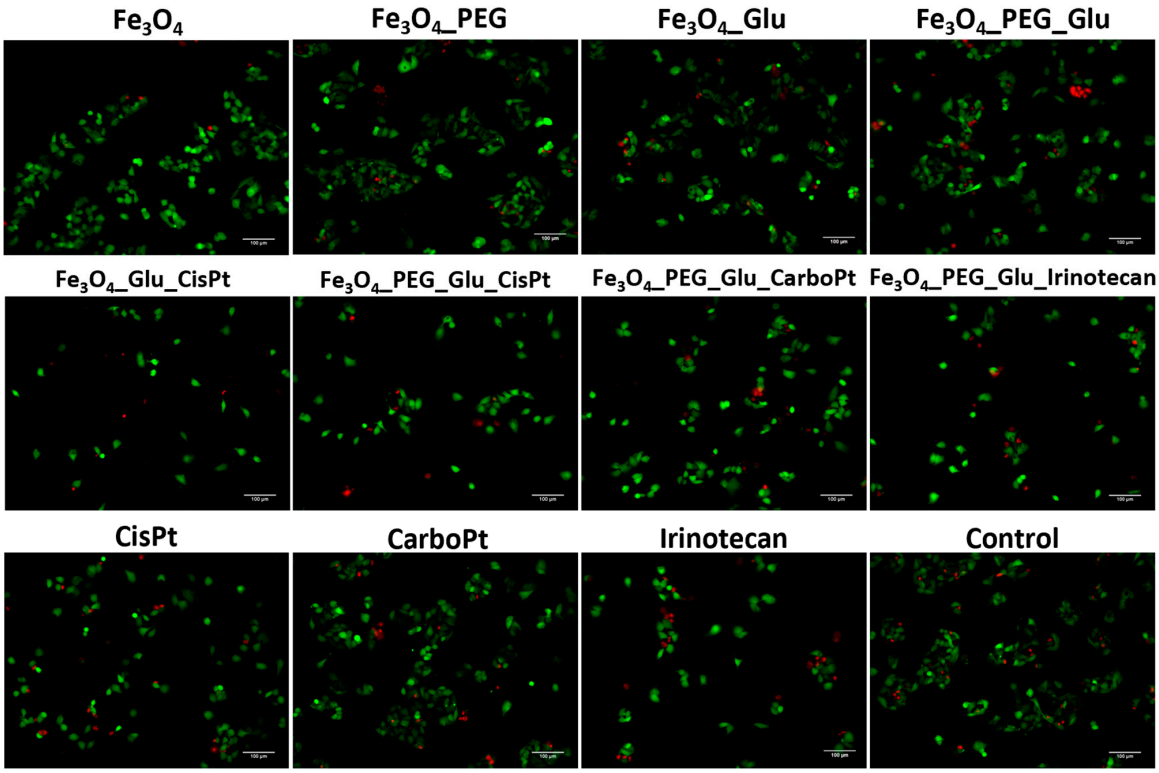

Figure 13. Live/Dead assay of HepG2 cells treated with drug-loaded MNP formulations and free drugs. Cytotoxic effects of various MNPs formulations and free drugs (CisPt, CarboPt, Irinotecan) were assessed in HepG2 cells following 24 h incubation at a concentration of 100 μg/mL, corresponding to 10 μg/mL of encapsulated drug. Viable cells are stained green with calcein-AM, while dead cells are stained red with propidium iodide. Scale bar: 100 μm.

A dose-dependent trend in AK release was noted for Fe_3O_4_PEG_Glu_CarboPt, with a noticeable increase at 500 μg/mL MNPs (equivalent to 50 μg/mL carboplatin). Nonetheless, the observed elevation in cytotoxicity did not achieve statistical significance (Figure 12E). Live/dead staining of HepG2 cells treated with 100 μg/mL Fe_3O_4_PEG_Glu_CarboPt revealed no significant difference in viability compared to untreated control cells (Figure 13). A statistically significant, concentration-dependent increase in adenylate kinase (AK) release was observed following treatment with free CarboPt, indicating enhanced cytotoxicity at higher doses. For irinotecan, both Fe_3O_4_PEG_Glu_Irinotecan and free irinotecan induced comparable and significant AK release after 24 h incubation with 100 and 500 μg/mL of MNPs, corresponding to 10 and 50 μg/mL of loaded drug, respectively (Figure 12F). These findings were corroborated by Live/Dead staining, which revealed a marked reduction in viable HepG2 cells upon treatment with 100 μg/mL Fe_3O_4_PEG_Glu_Irinotecan (equivalent to 10 μg/mL free irinotecan) (Figure 13). Notably, as shown in Figure 13, only a small number of cells remained adherent to the wells after 24 h of exposure to 100 μg/mL of cisplatin- and irinotecan-loaded MNPs, further confirming their potent cytotoxic effects at this concentration when loaded into the Fe_3O_4_Glu and Fe_3O_4_PEG_Glu carriers.

3.4. Cellular Uptake of MNPs

Iron staining by Prussian blue was used as a semi-quantitative method to assess the MNPs' internalization by hepatocytes after 24 h of incubation. HepG2 cells were treated with three concentrations (10, 100, and 500 μg/mL) of various MNP formulations and iron content was visualized using potassium ferrocyanide, with absorbance quantified at 700 nm (Figure 14A–C). All types of MNPs demonstrated dose-dependent internalization. However, no statistically significant differences were obtained among plain, PEGylated,

or Glu-functionalized MNPs, nor between plain and cisplatin-loaded MNPs, regardless of PEG surface modification (Figure 14A). Notably, Fe_3O_4_PEG_Glu_CarboPt exhibited significantly higher internalization at 10 µg/mL compared to Fe_3O_4 alone (Figure 14B), aligning with its pronounced anti-tumour efficacy in HepG2 cells. For irinotecan-loaded MNPs, no significant differences in uptake were detected at either 10 or 100 µg/mL (Figure 14C). At 500 µg/mL, nanoparticle clustering and adherence to the culture plate compromised quantification accuracy, rendering results at this concentration less reliable. To visualize individual MNP uptake via microscopy, a lower concentration of 5 µg/mL was used (Figure 14D).

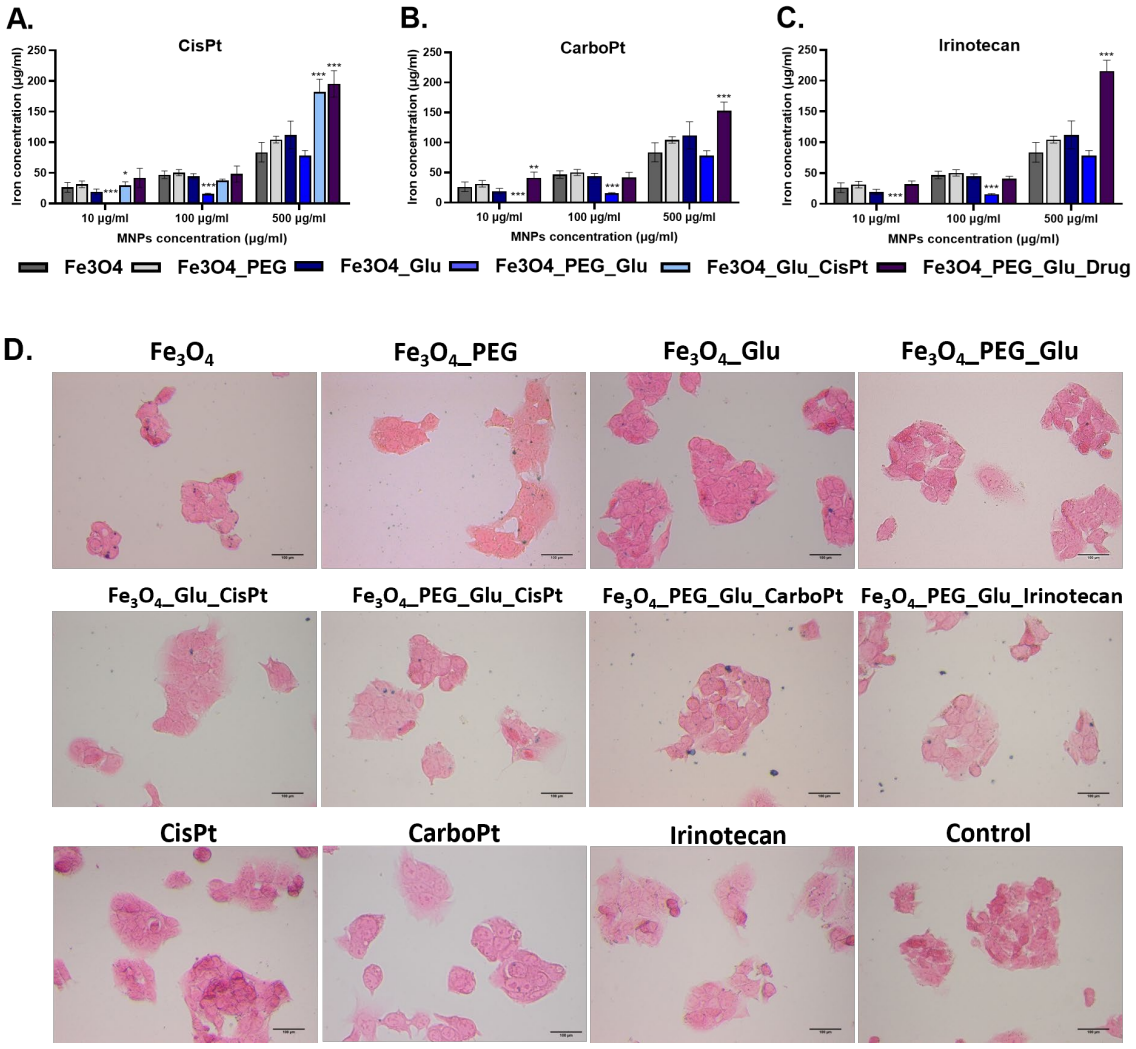

Figure 14. Evaluation of magnetic nanoparticle (MNP) internalization in HepG2 cells. Upper panel (**A**–**C**): Quantification of intracellular iron concentration following 24 h incubation with various MNP formulations loaded with cisplatin (**A**), carboplatin (**B**), or irinotecan (**C**), at concentrations of 10, 100, and 500 µg/mL. Iron was stained using potassium ferrocyanide, and absorbance was measured at 700 nm. Statistical significance is indicated relative to Fe_3O_4 nanoparticles: * $p < 0.05$, ** $p < 0.01$, *** $p < 0.001$. Lower panel (**D**): Bright-field microscopy images of HepG2 cells stained with Prussian blue after 24 h incubation with 5 µg/mL of MNPs loaded with cisplatin, carboplatin, or irinotecan. Untreated cells and cells exposed to free drugs (CisPt, CarboPt, Irinotecan) served as negative controls (with kind permission from the *Journal of the Australian Ceramic Society*, published by Springer Nature [12]). Scale bar: 100 µm.

The selection of the concentration (10, 100, and 500 µg/mL) of various MNPs was based considering that the surface functionalization of magnetic nanoparticles (MNPs) with PEG or glutamic acid alters their surface charge, hydrodynamic size, and interactions

with biomolecules in solution. Such physicochemical modifications are known to modulate cellular uptake pathways, including clathrin-mediated endocytosis, caveolae-dependent endocytosis, and macropinocytosis. For instance, PEGylation has been reported to reduce nonspecific interactions and facilitate uptake via caveolae and clathrin-mediated endocytosis [27]. In contrast, functionalization with negatively charged glutamic acid has been shown to favour caveolae-mediated internalization through specific receptor interactions, particularly ionotropic and metabotropic glutamate receptors [28]. These mechanistic differences may help explain the distinct intracellular accumulation patterns and cytotoxic responses observed in our formulations.

The cellular uptake was also evaluated by Scanning Transmission Electron Microscopy (STEM) as presented in Table 6. Comparative TEM analysis of magnetite nanoparticle formulations revealed distinct cellular interactions. Naked MNPs showed poor uptake and high aggregation, while PEG and glutamic acid coatings enhanced cellular uptake in a similar fashion, while clustering is slightly lower for the PEGylated MNPs. However, the glutamic acid coating determines a lower lysosomal activity than the PEG coating, meaning a better biocompatibility for glutamic acid-coated MNPs. The Fe_3O_4_PEG_Glu formulation achieved the most efficient cellular internalization with minimal stress responses, when compared to non-cisplatin formulations, implying that PEGylation is necessary for better stability, in order for a higher number of MNPs to reach their target [29]. PEGylation also allows for a higher load of active substances [27].

Table 6. Biodistribution and in vitro behaviour assessment of the magnetic nanoparticles within HepG2 cells by STEM analysis.

MNPs Name	Distribution	Observations
Fe_3O_4 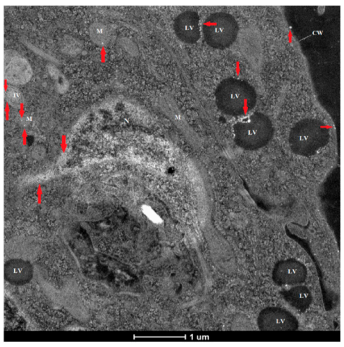 Figure T6.1.1. with kind permission from the ***Journal of the Australian Ceramic Society*** published by Springer Nature [8] 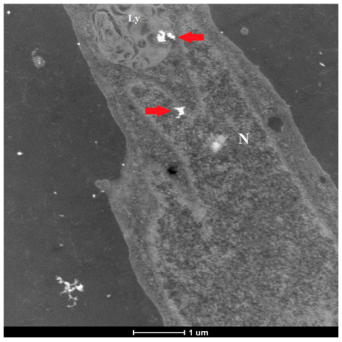 Figure T6.1.2.	- Few MNP clusters inside intracellular vesicles; - MNPs associated with the cell wall outside the cell; - MNPs inside the nucleus; - Some MNPs inside mitochondria; - MNPs associated with lipid vesicles; - MNP clusters formed on the outside of the cell wall; - Small clusters formed inside the nucleus; - MNPs cluster inside a lysosome.	- A 2 µm cluster of MNPs was observed within an intracellular vesicle, causing alterations to the cell's structure and ultrastructure. - Although some MNPs were adsorbed or internalized within various cellular organelles, the majority remained accumulated at the cell wall barrier, indicating limited uptake of the uncoated MNPs.

Table 6. *Cont.*

MNPs Name	Distribution	Observations
Fe_3O_4_PEG 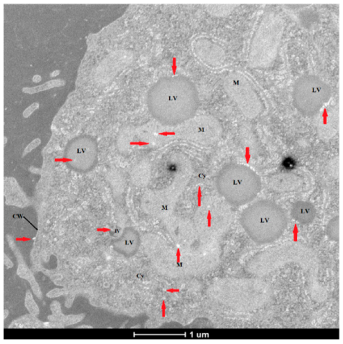 Figure T6.2. with kind permission from the ***Journal of the Australian Ceramic Society*** published by Springer Nature, [8]	- MNPs associated with lipid vesicles; - Numerous MNPs inside mitochondria; - MNPs in the cytoplasm; - MNPs inside intracellular vesicles; - Few MNPs associated with the cell wall outside the cell; - Some MNPs inside the nucleus; - MNPs cluster inside a lysosome; - Small MNPs cluster inside mitochondria.	- MNPs were detected in all organelles, similar to the Fe_3O_4 sample. However, the distribution suggests that a greater number of MNPs successfully penetrated the cell wall and interacted with intracellular organelles compared to the uncoated MNPs. Fewer individual MNPs or clusters were observed associated with the cell membrane. - TEM analysis revealed that the Fe_3O_4_PEG formulation exhibited a higher efficiency of cellular internalization than the uncoated MNPs.
Fe_3O_4_Glu 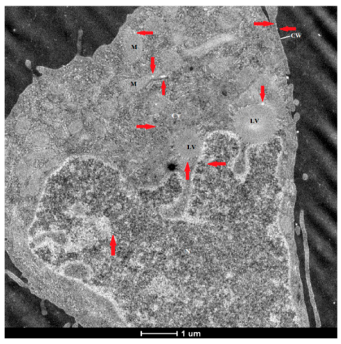 Figure T6.3.	- Numerous MNPs associated with lipid vesicles; - Small and large MNP clusters inside mitochondria; - Few small MNP clusters on the outside of the cell wall; - Numerous MNPs inside the nucleus; - Free MNPs inside the cytoplasm; - Few large MNP clusters inside the nucleus.	- MNPs were abundantly observed within the cells, with only a few clusters associated with the cell wall. This suggests that the Fe_3O_4_Glu formulation exhibits high cellular penetration, comparable to the Fe_3O_4_PEG formulation and greater than that of the uncoated MNPs. Additionally, the MNPs appeared to be uniformly distributed throughout the cell. - Moreover, there are few clusters of small dimensions (under 200 nm) which present a lower grade of aggregation for the Fe_3O_4_Glu MNP formulation.
Fe_3O_4_PEG_Glu 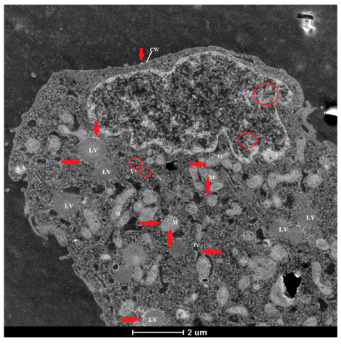 Figure T6.4.	- MNPs are present abundantly in the nucleus; - MNPs are present abundantly in mitochondria; - Few MNP clusters are associated with lipid vesicles; - Numerous MNPs free in the cytoplasm; - Few MNPs associated with the cell wall; - Cells present no lysosome; - Few MNPs are found in intracellular vesicles.	- The Fe_3O_4_PEG_Glu formulation exhibited the lowest degree of aggregation among all tested samples, with only a few MNP clusters observed either inside or outside the cells. - Within the cells, MNPs were uniformly distributed and abundantly present across all organelles—at even higher levels than in the Fe_3O_4_Glu and Fe_3O_4_PEG formulations. Very few MNPs were detected near the cell walls, suggesting that the Fe_3O_4_PEG_Glu formulation demonstrated superior cellular uptake and was able to efficiently penetrate both the cell wall and intracellular membranes. - Furthermore, the absence of lysosomal accumulation indicates that the cells were able to metabolize the MNPs without eliciting a pronounced defensive or stress response.

Table 6. *Cont.*

MNPs Name	Distribution	Observations
Fe_3O_4_Cisplatin 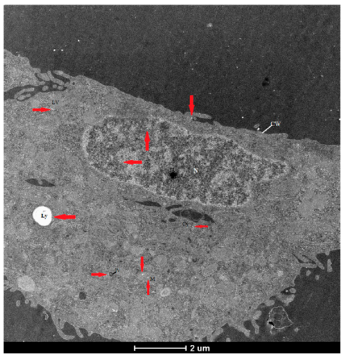 Figure T6.5.	- Few MNPs associated with the cell wall outside the cell; - MNPs inside mitochondria; - MNPs inside the nucleus; - MNPs associated with lipid vesicles; - Some MNPs inside mitochondria and cytoplasm; - MNPs inside lysosomes; - Few MNPs accumulated inside intracellular vesicles.	- MNPs reached all cellular organelles, similar to the other formulations, but in smaller quantities. The MNPs appeared to behave differently, eliciting distinct cellular responses. The Fe_3O_4_CisPt nanoparticles exhibited a markedly lower tendency to form clusters or aggregates, resulting in a more uniform intracellular distribution. - The Fe_3O_4_CisPt-treated samples showed a high proportion of dead cells, likely due to the rapid release of cisplatin. However, the surviving cells displayed an increased number of lysosomes compared to those treated with other formulations, indicating enhanced lysosomal activity. This suggests that the Fe_3O_4_CisPt nanoparticles were not metabolized but instead targeted for degradation or exocytosis. Consequently, it can be inferred that only cells with elevated lysosomal activity survived the treatment and were imaged prior to cell death; these surviving cells formed the basis of the analysis.
Fe_3O_4_Glu_Cisplatin 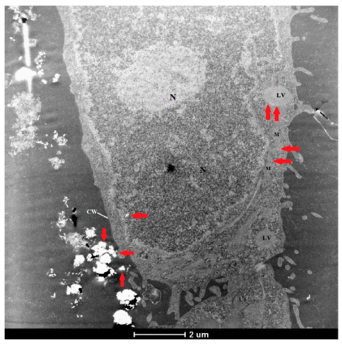 Figure T6.6.1. 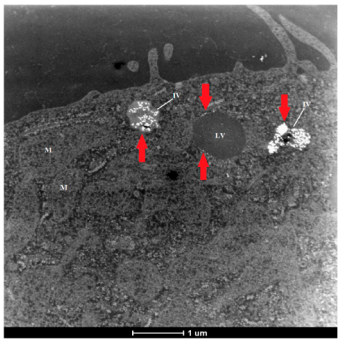 Figure T6.6.2.	- Small and large MNP clusters associated with cell walls; - Large MNP clusters (1 to 2 µm) inside intracellular vesicles; - Small clusters inside intracellular vesicles; - Few small MNP clusters inside the nucleus; - Some MNPs inside the nucleus; - Few MNPs associated with lipid vesicles; - Some MNPs inside mitochondria; - Few MNPs free in the cytoplasm; - Few lysosomes present.	- The Fe_3O_4_Glu_CisPt formulation exhibited a strong tendency to form aggregates, including both small and predominantly large clusters (1–2 µm in size). The number of MNPs that successfully penetrated the cells was lower than in all other formulations, likely due to the larger aggregate size. - Both the Fe_3O_4_Glu_CisPt and Fe_3O_4_CisPt formulations showed a high proportion of dead cells in the analyzed samples, suggesting that the surviving cells were those with reduced nanoparticle uptake or lower susceptibility. - However, compared with the Fe_3O_4_CisPt formulation, the Fe_3O_4_Glu_CisPt formulation displayed significantly fewer lysosomes, indicating that it partially suppresses the cellular defensive response, despite the nanoparticles ultimately leading to cell death.

Table 6. *Cont.*

MNPs Name	Distribution	Observations
Fe_3O_4_PEG_Glu_Cisplatin 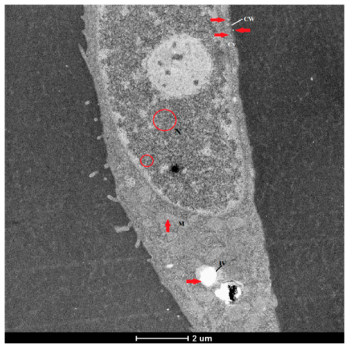 Figure T6.7.1. 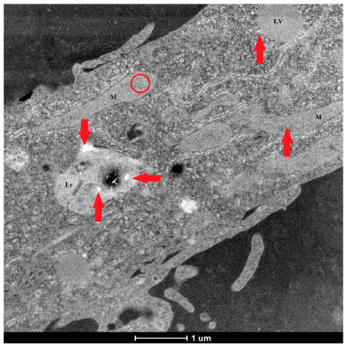 Figure T6.7.2.	- Large MNP clusters (1 to 2 µm) inside intracellular vesicles; - Numerous MNPs inside the nucleus; - MNPs abundantly present in mitochondria and cytoplasm; - Few MNPs at cell wall level; - Few large MNP clusters outside the cell; - Small MNP clusters inside mitochondria; - MNPs associated with lipid vesicles; - MNPs inside lysosomes.	- The Fe_3O_4_PEG_Glu_CisPt formulation demonstrated high cellular uptake, with only the larger clusters remaining unable to cross the cell wall. Although it formed sizable aggregates, their incidence was lower than in the Fe_3O_4_Glu_CisPt formulation, which did not appear to compromise the formulation's overall efficacy. This formulation effectively induced cell death, as evidenced by the substantial number of dead cells observed in the samples. - A considerable portion of the internalized MNPs was metabolized within intracellular vesicles and lysosomes, reflecting the extensive nanoparticle uptake. The Fe_3O_4_PEG_Glu_CisPt formulation successfully reached most cellular organelles, with a lower association with lipid vesicles and predominant localization within the mitochondria, cytoplasm, and nucleus. - Although this formulation triggered a defensive response—characterized by lysosomal activity and intracellular encapsulation—unlike the Fe_3O_4_PEG_Glu formulation, this reaction was not universal across all penetrated cells. The response appeared to result from both the high intracellular concentration of MNPs and the presence of cisplatin. - Overall, the Fe_3O_4_PEG_Glu_CisPt formulation combines the key characteristics of its individual components, effectively balancing their advantages and limitations. It exhibits strong cellular compatibility, reduced nanoparticle aggregation, and efficient cisplatin release in most cells, while eliciting only moderate defensive responses.

Red arrows and red circles indicate MNPs or MNP clusters. IV—intracellular vesicles; CW—cell wall; N—nucleus; M—mitochondria; LV—lipid vesicles; Cy—cytoplasm; Ly—lysosome.

When loaded with cisplatin, nanoparticles exhibited increased cytotoxicity, aggregation and lysosomal activity. Among drug-loaded systems characterized by STEM, Fe_3O_4_PEG_Glu_CisPt displayed the best balance of high uptake, effective drug release, moderate to low aggregation, and limited defensive responses, making it the most promising formulation for intracellular delivery and therapeutic applications. Fe_3O_4_PEG_Glu_CisPt formulation demonstrates the most balanced performance, optimizing cell penetration, drug release, and biocompatibility.

4. Conclusions

Magnetic nanoparticles are highly promising in theranostics, being able to sustain a multimodal therapy in a targeted approach if proper surface modification is implemented. Novel drug delivery systems with improved internalization capacity, based on PEG-stabilized magnetic nanoparticles and further functionalized with glutamic acid, were obtained and tested as carriers for anticancer drugs. These MNPs were found to be preferentially internalized into the tumour cells, while the decrease in the survival rate of the cells treated with the drug delivery systems vs. free-drug-treated cells suggests a higher cellular uptake and an improved therapeutic efficiency. As perspectives, we are aiming to evaluate these MNPs as a multifunctional system with the capability to trigger hyperthermia by external magnetic fields. In this way, a more efficient therapy could be assured based on the preferentially internalization into the tumour cells followed by magnetically triggered cytostatic release. Based on the obtained results, it was found that glutamic acid can improve the internalization efficiency of the magnetic carriers, even if loaded with antitumoral agents, these systems acting as veritable Trojan horses in targeted cancer therapy. Furthermore, by integrating imaging capabilities of the MNPs with the delivery path presented above, these systems can provide a comprehensive approach in cancer therapy, significantly impacting future clinical applications and patient outcomes. Such systems can have a triggered or a programmed release of the antitumoral drugs, as hyperthermia can be generated after a predefined time or after imaging techniques indicate a good accumulation of the MNPs in the targeted tissue. Further optimization of these systems is needed and tested at in vitro level followed by the in vivo evaluation of these systems on specific types of cancer, but also, these studies will be extended to magnetic guidance for nerve regeneration or as carriers in vaccine formulations.

Author Contributions: Conceptualization, A.F., O.-C.O. and D.F.; validation, O.-C.O. and A.F.; investigation, M.C., D.S.M., L.M., G.V., M.A., V.-A.S., O.-C.O., V.-E.P., B.S.V. and R.D.T.; resources, D.F. and O.-C.O.; writing—original draft preparation, V.-E.P., D.S.M., A.S., B.S.V., G.V.,L.M., M.A., M.C., V.-A.S., D.F. and O.-C.O.; writing—review and editing, A.F., V.-E.P., A.S., D.F., M.C., G.V., M.A. and L.M.; visualization, L.M., D.F., M.C., A.F. and O.-C.O.; supervision, V.-E.P., M.C., O.-C.O., A.F. and D.F. All authors have read and agreed to the published version of the manuscript.

Funding: The authors acknowledge the support of the Flag Era project, "Smart nerve Grafts based on Graphene-related composite materials with electric-triggering capability for central and peripheral nervous system regeneration" [SMART2GRAPH], co-funded by the Ministry of Research, Innovation and Digitization, CNCS/CCCDI-UEFISCDI, project number 28/17.05.2024, as well as by the Romanian Government, for providing access to the research infrastructure of the National Centre for Micro and Nanomaterials through the National Program titled "Installations and Strategic Objectives of National Interest.

Data Availability Statement: The original contributions presented in this study are included in the article. Further inquiries related to specific formats or additional data can be directed to the corresponding author.

Conflicts of Interest: The authors declare no conflict of interest.

References

1. Zhao, J.; Xu, L.; Sun, J.; Song, M.; Wang, L.; Yuan, S.; Zhu, Y.; Wan, Z.; Larsson, S.; Tsilidis, K.; et al. Global trends in incidence, death, burden and risk factors of early-onset cancer from 1990 to 2019. *BMJ Oncol.* **2023**, *2*, e000049. [CrossRef]
2. Yahya, S.; Pushpanathan, S.; Jan, S.; Chaudhary, N.; Parray, R.; Gandhi, K.A.; Thangavel, K.; Krishnan, K.; Sudhandiran, G. Development and characterization of pegylated Fe_3O_4-CAPE magnetic nanoparticles for targeted therapy and hyperthermia treatment of colorectal cancer. *Sci. Rep.* **2025**, *15*, 26008. [CrossRef]
3. Wang, Y.; Liu, X.; Ma, S.; He, X.; Guo, C.; Liang, Z.; Hu, Y.; Wei, Y.; Lian, X.; Huang, D. Progress in cancer therapy with functionalized Fe_3O_4 nanomaterials. *Front. Mater. Sci.* **2023**, *17*, 230658. [CrossRef]
4. Winkler, R.; Ciria, M.; Ahmad, M.; Plank, H.; Marcuello, C. A Review of the Current State of Magnetic Force Microscopy to Unravel the Magnetic Properties of Nanomaterials Applied in Biological Systems and Future Directions for Quantum Technologies. *Nanomaterials* **2023**, *13*, 2585. [CrossRef] [PubMed]
5. Li, Q.; Kartikowati, C.W.; Horie, S.; Ogi, T.; Iwaki, T.; Okuyama, K. Correlation between particle size/domain structure and magnetic properties of highly crystalline Fe_3O_4 nanoparticles. *Sci. Rep.* **2017**, *7*, 9894. [CrossRef]
6. Ebadi, M.; Zain, A.R.M.; Aziz, T.H.T.A.; Mohammadi, H.; Tee, C.A.T.; Yusop, M.R. Formulation and Characterization of Fe_3O_4@PEG Nanoparticles Loaded Sorafenib; Molecular Studies and Evaluation of Cytotoxicity in Liver Cancer Cell Lines. *Polymers* **2023**, *15*, 971. [CrossRef] [PubMed]
7. Thong, P.Q.; Huong, L.T.T.; Tu, N.D.; Nhung, H.T.M.; Khanh, L.; Manh, D.H.; Nam, P.H.; Phuc, N.X.; Alonso, J.; Qiao, J.; et al. Multifunctional nanocarriers of Fe_3O_4@PLA-PEG/curcumin for MRI, magnetic hyperthermia and drug delivery. *Nanomedicine* **2022**, *17*, 1677–1693. [CrossRef]
8. Elbeltagi, S.; Shakor, A.B.A.; Alharbi, H.M.; Tawfeek, H.M.; Aldosari, B.N.; Eldin, Z.E.; Amin, B.H.; El-Aal, M.A. Synergistic effects of quercetin-loaded $CoFeO_4$@Liposomes regulate DNA damage and apoptosis in MCF-7 cancer cells: Based on biophysical magnetic hyperthermia. *Drug Dev. Ind. Pharm.* **2024**, *50*, 561–575. [CrossRef]
9. Elbeltagi, S.; Madkhali, N.; Alharbi, H.M.; Eldin, Z.E. MXene-encapsulated ZIF-8@Liposomes for NIR-enhanced photothermal therapy in hepatocellular carcinoma treatment: In vitro, in vivo, and in silico study. *Arch. Biochem. Biophys.* **2025**, *764*, 110256. [CrossRef]
10. Hajba, L.; Guttman, A. The use of magnetic nanoparticles in cancer theranostics: Toward handheld diagnostic devices. *Biotechnol. Adv.* **2016**, *34*, 354–361. [CrossRef]
11. Chauhan, A.; Kumar, R.; Singh, P.; Jha, S.K.; Kuanr, B.K. RF hyperthermia by encapsulated Fe_3O_4 nanoparticles induces cancer cell death via time-dependent caspase-3 activation. *Nanomedicine* **2020**, *15*, 355–379. [CrossRef]
12. Motelica, L.; Voicu, G.; Chircov, C.; Surdu, A.V.; Trusca, R.D.; Vasile, B.S.; Ficai, D.; Oprea, O.C.; Marta, D.S.; Peteu, V.-E.; et al. Aspartic acid functionalized magnetic nanoparticles for enhanced internalization in tumoral cell. *J. Aust. Ceram. Soc.* **2025**, *61*, 265–283. [CrossRef]
13. Dutta, S.; Ray, S.; Nagarajan, K. Glutamic acid as anticancer agent: An overview. *Saudi Pharm. J.* **2013**, *21*, 337–343. [CrossRef] [PubMed]
14. Turtoi, M.; Anghelache, M.; Bucatariu, S.-M.; Deleanu, M.; Voicu, G.; Safciuc, F.; Manduteanu, I.; Fundueanu, G.; Simionescu, M.; Calin, M. A novel platform for drug testing: Biomimetic three-dimensional hyaluronic acid-based scaffold seeded with human hepatocarcinoma cells. *Int. J. Biol. Macromol.* **2021**, *185*, 604–619. [CrossRef] [PubMed]
15. Anghelache, M.; Turtoi, M.; Petrovici, A.R.; Fifere, A.; Pinteala, M.; Calin, M. Development of Dextran-Coated Magnetic Nanoparticles Loaded with Protocatechuic Acid for Vascular Inflammation Therapy. *Pharmaceutics* **2021**, *13*, 1414. [CrossRef]
16. Junejo, Y.; Baykal, A.; Sözeri, H. Simple hydrothermal synthesis of Fe_3O_4-PEG nanocomposite. *Open Chem.* **2013**, *11*, 1527–1532. [CrossRef]
17. Almeida, P.B.; Pinatti, I.M.; de Oliveira, R.C.; Teixeira, M.M.; Santos, C.C.; Machado, T.R.; Longo, E.; Rosa, I.L.V. Structural, morphological and photoluminescence properties of β-Ag_2MoO_4 doped with Eu^{3+}. *Chem. Pap.* **2021**, *75*, 1869–1882. [CrossRef]
18. Zhao, D.-L.; Teng, P.; Xu, Y.; Xia, Q.-S.; Tang, J.-T. Magnetic and inductive heating properties of Fe_3O_4/polyethylene glycol composite nanoparticles with core-shell structure. *J. Alloys Compd.* **2010**, *502*, 392–395. [CrossRef]
19. Covaliu, C.I.; Jitaru, I.; Paraschiv, G.; Vasile, E.; Biriş, S.; Diamandescu, L.; Ionita, V.; Iovu, H. Core-shell hybrid nanomaterials based on $CoFe_2O_4$ particles coated with PVP or PEG biopolymers for applications in biomedicine. *Powder Technol.* **2013**, *237*, 415–426. [CrossRef]
20. Li, H.; Tripp, C.P. Infrared study of the interaction of charged silica particles with TiO particles containing adsorbed cationic and anionic polyelectrolytes. *Langmuir* **2005**, *21*, 2585–2590. [CrossRef]
21. Ficai, D.; Ficai, A.; Vasile, B.S.; Ficai, M.; Oprea, O.; Guran, C.; Andronescu, E. Synthesis of Rod-Like Magnetite by Using Low Magnetic Field. *Dig. J. Nanomater. Biostructures* **2011**, *6*, 943–951.
22. Chircov, C.; Ștefan, R.-E.; Dolete, G.; Andrei, A.; Holban, A.M.; Oprea, O.-C.; Vasile, B.S.; Neacșu, I.A.; Tihăuan, B. Dextran-Coated Iron Oxide Nanoparticles Loaded with Curcumin for Antimicrobial Therapies. *Pharmaceutics* **2022**, *14*, 1057. [CrossRef]

23. Movileanu, C.; Anghelache, M.; Turtoi, M.; Voicu, G.; Neacsu, I.A.; Ficai, D.; Trusca, R.; Oprea, O.; Ficai, A.; Andronescu, E.; et al. Folic acid-decorated PEGylated magnetite nanoparticles as efficient drug carriers to tumor cells overexpressing folic acid receptor. *Int. J. Pharm.* **2022**, *625*, 122064. [CrossRef]
24. Chircov, C.; Matei, M.-F.; Neacșu, I.A.; Vasile, B.S.; Oprea, O.-C.; Croitoru, A.-M.; Trușcă, R.-D.; Andronescu, E.; Sorescu, I.; Bărbuceanu, F. Iron Oxide-Silica Core-Shell Nanoparticles Functionalized with Essential Oils for Antimicrobial Therapies. *Antibiotics* **2021**, *10*, 1138. [CrossRef]
25. Caciandone, M.; Niculescu, A.-G.; Roșu, A.R.; Grumezescu, V.; Negut, I.; Holban, A.M.; Oprea, O.; Vasile, B.Ș.; Bîrcă, A.C.; Grumezescu, A.M.; et al. PEG-Functionalized Magnetite Nanoparticles for Modulation of Microbial Biofilms on Voice Prosthesis. *Antibiotics* **2022**, *11*, 39. [CrossRef] [PubMed]
26. Gherasim, O.; Popescu, R.C.; Grumezescu, V.; Mogoșanu, G.D.; Mogoantă, L.; Iordache, F.; Holban, A.M.; Vasile, B.Ș.; Bîrcă, A.C.; Oprea, O.-C.; et al. MAPLE Coatings Embedded with Essential Oil-Conjugated Magnetite for Anti-Biofilm Applications. *Materials* **2021**, *14*, 1612. [CrossRef]
27. Digiacomo, L.; Renzi, S.; Pirrottina, A.; Amenitsch, H.; De Lorenzi, V.; Pozzi, D.; Cardarelli, F.; Caracciolo, G. PEGylation-Dependent Cell Uptake of Lipid Nanoparticles Revealed by Spatiotemporal Correlation Spectroscopy. *ACS Pharmacol. Transl. Sci.* **2024**, *7*, 3004–3010. [CrossRef] [PubMed]
28. Francesconi, A.; Kumari, R.; Zukin, R.S. Regulation of Group I Metabotropic Glutamate Receptor Trafficking and Signaling by the Caveolar/Lipid Raft Pathway. *J. Neurosci.* **2009**, *29*, 3590–3602. [CrossRef] [PubMed]
29. Karimova, A.; Hajizada, S.; Shirinova, H.; Nuriyeva, S.; Gahramanli, L.; Mehdiyeva, A.; Eyvazova, G.; Sadikhov, T.; Lenz, N.; Nasirova, I.; et al. Dextran-coated Fe_3O_4 nanoparticles with ratio-dependent drug loading: Structural characterization and cytotoxicity in colorectal cancer cells. *Front. Nanotechnol.* **2025**, *7*, 1634225. [CrossRef]